12

Elastic and plastic deformation in nanocrystalline metals

M.Y. GUTKIN, Russian Academy of Sciences, Russia

Abstract: This chapter discusses theoretical models that describe structure, elastic strains and different mechanisms of strain relaxation and plastic deformation of nanocrystalline metals. Special attention is paid to structure, strained state and the pentagonal symmetry of nanoparticles, in which context the disclination models and channels of strain relaxation are reviewed. For nanocrystalline metals, various grain boundary stress sources and concentrators are examined with regard to their capacity to initiate the mechanisms of plastic deformation. Theoretical modeling of dislocation generation, deformation twinning, rotational and superplastic deformation, and athermal stress-induced grain growth is considered in detail.

Key words: strained state in nanoparticles, mechanisms of plasticity in nanocrystalline metals, generation of dislocations and twins, rotational and superplastic deformation, athermal stress-induced grain growth.

12.1 Introduction

Outstanding mechanical properties of nanocrystalline metals (NCMs) have attracted much attention since the end of the 1980s when first NCMs had been fabricated and studied. In particular, it became at once clear that the behavior of defects and mechanisms of plastic deformation in NCMs and conventional polycrystalline metals are rather different.[1,2] However, the experimental study of defects in NCMs has met many difficulties, which determines the importance of theoretical modeling and computer simulations. This chapter reviews some analytical theoretical models that describe deformation phenomena in NCMs. Section 12.2 is devoted to elastic strains in as-fabricated NCMs. Our view is that understanding the initial strained state should be considered as the first and necessary step in modeling the deformation processes in NCMs. Moreover, the assumptions on the elastic-state characteristics of a representative NCM volume form the basis of the majority of theoretical models describing various mechanisms of plastic deformation and fracture in NCMs. That is why we pay much attention to elastic strains here. Starting from peculiarities of elastic-strain distribution and relaxation in isolated nanoparticles and their conglomerates, we then briefly consider grain boundary (GB) stress sources and concentrators in NCMs. In the stress fields of these GB sources and concentrators, various mechanisms of plastic deformation can start working, including dislocation emission from GBs, generation of deformation twins, GB migration, transformation and decay, etc.

Theoretical models of these mechanisms are considered in Section 12.3. Then in the same section the interplay between translational and rotational modes of plastic deformation is discussed together with mechanisms that provide local changes in misorientation angles of GBs and can result in grain rotation. The theoretical models, which describe the effects of strengthening and softening of NCMs under superplastic deformation, are also reviewed there. It is demonstrated that most of the models under discussion can be analysed within a unified energy approach, where some critical values of parameters (for example, a critical value of the applied shear stress) are calculated to state the conditions necessary for the barrierless activation of the deformation mechanisms. When possible, theoretical estimates are compared with available experimental data that allows one to conclude that the model is either realistic or is not.

12.2 Elastic strains in nanocrystalline metals

As-fabricated NCMs are always the subject of residual elastic strains. For example, Wunderlich *et al*.[3] evaluated one of the first transmission electron microscopy (TEM) studies of a NCM (nc-Pd with the grain size of 4–9 nm, which was fabricated by high-pressure compaction of nanocrystallites condensed from the gas phase) and showed that many GBs have severely distorted near-boundary regions with smaller atomic density and higher level of elastic strains. In general, their sample contained about 25% of highly strained material. Similar conclusions followed from comparison of earlier experimental data from Mössbauer spectroscopy,[4] positron lifetime spectroscopy,[5,6] X-ray diffraction,[7] EXAFS[8] and neutron diffraction.[9] Later, in the middle of the 1990s, residual elastic strains were investigated in detail in NCMs obtained by severe plastic deformation.[10] The general result was that the elastic strains were distributed inhomogeneously over the grains: they reached their maximum values in the vicinity of GBs and demonstrated an exponential slope at a distance of several nanometers from the GBs. To understand the origin of the residual elastic strains in NCMs, it is reasonable to start from the main features of NCM structure.

Usually NCMs consist of crystalline grains (ranging from several to approximately one hundred nanometers in diameter), which are separated by GBs. The GBs meet each other at linear junctions that are called double if two GBs meet, triple if three GBs meet, etc. In their turn, the GB junctions meet each other at point nodes, which can be fourfold, fivefold, etc. Most GB junctions and their nodes are triple and fourfold, respectively. Their total volume fraction drastically increases with grain refinement and can reach up to 50% in fine-grained NCMs.[1] As follows from these structural peculiarities of NCMs, there are two main reasons for their unique mechanical and physical properties: the first one is the nanoscopic grain size, and the second one is the unusually high density of GBs, GB junctions and junction nodes. Let us first consider the origin of residual elastic strains in isolated nanoparticles (or nanoclusters) and then in their conglomerates.

12.2.1 Nanoparticles

Residual elastic strains appear in isolated nanoparticles due to various reasons such as surface stress, pentagonal symmetry, presence of defects, phase transformations, etc.

The physical origin of the surface stress is that the chemical bonding of atoms at the crystal surface is different from the bonding of atoms in the crystal bulk.[11] Therefore, the equilibrium distance between the surface atoms differs from that between the bulk atoms, and the subsurface atomic layers occur in elastically strained state. For an isotropic spherical nanoparticle of radius R, there is a rough estimate of the average distortion of the interatomic distance a caused by surface tension that reads[2,12]:

$$\frac{\Delta a}{a} \approx \frac{2}{3} K \frac{\gamma}{R}, \qquad [12.1]$$

where K is the volume compressibility coefficient and γ is the specific surface energy. For typical values of parameters $K \sim 10^{-11}$ m^3/J, $\gamma \sim 1$ J/m^2 and $R \sim 10$ nm, this estimate gives approximately, $0.67 \cdot 10^{-3}$, that is about one-tenth of a percent.[2] It has also been noted that parameters entering equation [12.1] are size dependent.[2] In particular, the surface energy of a nanoparticle depends on its radius R as[13]

$$\gamma = \gamma_0 \left\{ 1 - \alpha \frac{a}{R} + \beta \left(\frac{a}{R} \right)^2 + \ldots \right\}, \qquad [12.2]$$

where γ_0 is the specific surface energy of a bulk crystal, $\alpha \approx 1$ and $\beta \approx \alpha^2 \approx 1$ are numerical coefficients. Thus, the surface energy γ decreases with decreasing nanoparticle radius R. It is worth noting that the surface energy of nanoparticles also decreases with increasing temperature (see, for example, Jia *et al.*[14] and references therein). Nevertheless, equation [12.1] demonstrates the main contribution of radius R to the elastic strains caused by the surface stress in nanoparticles.

The majority of isolated nanoparticles are synthesized in the single crystalline state;[15] however, they also demonstrate a large variety of structures and shapes. 'The next most common structure is probably simple twins, although there is rarely any publication of statistical data of particle populations. Of rather lower probability except for gold and silver is multiply twinned particles' (Marks,[15]). Among the multiply twinned particles, fivefold-twinned nano- and microparticles have attracted much attention due to their pentagonal symmetry, which is impossible in bulk single crystalline solids (see, for example, the reviews[2,15–22] and recent papers).[23–26] Fivefold-twinned nanoparticles can have shapes close to regular decahedra, icosahedra or pentagonal prisms.

De Wit[27] and Galligan[28] independently pointed out a direct relation between the structure of fivefold-twinned nanoparticles and disclinations (see also[2,19,29]). For illustration, de Wit[27] suggested considering the undeformed body, which consists

of five face-centered cubic (FCC) crystals oriented with the $(1\ \bar{1}\ 0)$ plane in the plane of the paper (Fig. 12.1 (a)). Each crystal is in twin orientation with respect to the adjacent one, so that AC, AD, AE, and AF are twin boundaries. The angle between each pair of (1 1 1) and $(\bar{1}\ \bar{1}\ 1)$ planes is 70°32′. Therefore the resulting polycrystal has a wedge BAB′ with an apex angle of 7°20′. If the two sides of this wedge are brought together they will form a twin boundary, while at the same time a positive wedge disclination is created at A, where five twin boundaries terminate (Fig. 12.1 (b)). Thus, the final configuration has no wedge-like cusp BAB′ but contains a partial disclination of strength $\omega = 7°20'$, which creates inhomogeneous elastic strains and stresses in the polycrystal.

In the case of decahedral nanoparticles (Fig. 12.2 (a)) or pentagonal rods (Fig. 12.2 (b)), there is only one such 'star disclination' whose line coincides with the pentagonal symmetry axis.[27] In icosahedral nanoparticles, there are six such disclinations whose lines pass through twelve icosahedron vertices (Fig. 12.2 (c), see Ref. 19 for details).

The idea to use the disclination concept has been very productive because it gives a straightforward way of modeling the elastic strains and stresses in fivefold-twinned nanoparticles. For example, de Wit[27] approximated the decahedral nanoparticle by a section of a cylinder containing a wedge disclination of strength ω along its axis. In this case the non-vanishing stress components (in cylindrical coordinates r, φ and z) read:

$$\sigma_{rr} = D\omega \ln\frac{r}{R}, \quad \sigma_{\varphi\varphi} = D\omega\left(\ln\frac{r}{R}+1\right), \quad \sigma_{zz} = D\nu\omega\left(2\ln\frac{r}{R}+1\right), \quad [12.3]$$

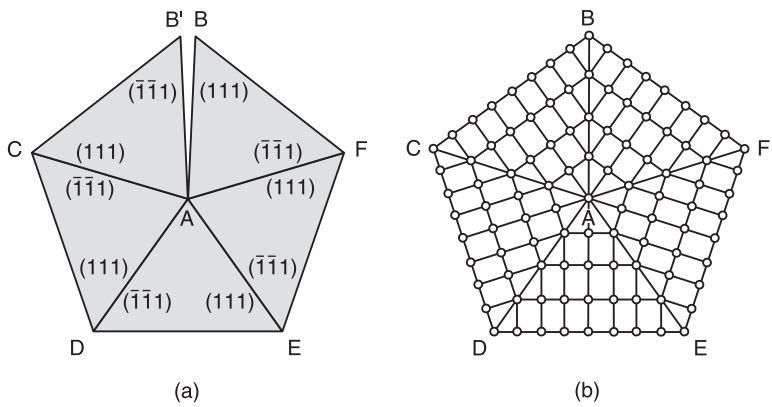

12.1 De Wit's schematics[27] of partial disclination formation in the core of a fivefold twin in FCC crystals. (a) Initial undeformed state of a polycrystal consisting of five FCC crystals, each in twin orientation with respect to its neighbour; the plane of the paper is $(1\ \bar{1}\ 0)$ and AC, AD, AE, and AF are twin boundaries. (b) A positive partial wedge disclination at A on which terminate the five twin boundaries AB, AC, AD, AE, and AF.

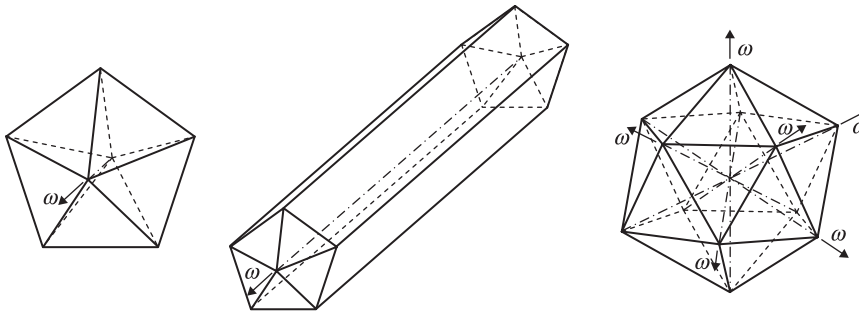

12.2 Partial positive wedge disclinations of strength ω in (a) decahedral nanoparticle, (b) pentagonal rod, and (c) icosahedral nanoparticle.

where $D = G/[2\pi(1-\nu)]$, G is the shear modulus, ν is the Poisson ratio, and R is the cylinder radius. It is seen from equation [12.3] that the central region of the nanoparticle is compressed while its periphery is stretched. Indeed, the hydrostatic stress component $\sigma = 1/3\mathrm{Tr}\sigma_{ij} = 1/3\, D\omega(1+\nu)[2\ln(r/R)+1]$, is negative at $r < 0.6R$, zero at $r \approx 0.6R$ and positive at $r > 0.6R$. The stresses are singular at $r = 0$, which is a generic feature of solutions for defects (like cracks, dislocations, disclinations, etc.) within the classical theory of elasticity. Using an extended version of the elasticity theory (say, the strain-gradient,[30,31] non-local[32] or non-linear[33] theory of elasticity), one can dispense with such singularities. For example, in the framework of the strain-gradient elasticity, the hydrostatic stress component at the line of a positive wedge disclination, which is placed at the distance ~ 1 μm from a negative wedge disclination of the same strength, is estimated as[30,31] $\sigma \approx -6D\omega(1+\nu)$, which gives $\sigma \sim -D \sim -G/4$ for $\omega = 7°20' \approx 0.128$ and $\nu = 0.3$. Lazar[34] has used the field theory of elastoplasticity to consider a wedge disclination in the center of a cylinder of radius R and obtained $\sigma \approx -1.14D\omega(1+\nu)$ at the dislocation line for $R = 10/\kappa$, where κ is the gradient coefficient, which can be estimated as ~ 10 nm^{-1}. Then we get $\sigma \sim -D/5 \sim -G/20$ for R ~ 1 nm at the same values of ω and ν. Thus, the level of $G/20$ can be considered as the lower magnitude of σ in the finest nanoparticles, while $G/4$ as its upper magnitude in the coarse nanoparticles. Anyway, the compression in the nanoparticle center is very high. Moreover, it follows from equation [12.3] that the strain energy (per unit disclination length) is[27] $W_{Dh} = 1/8D\omega^2R^2$. Therefore, one can expect the activation of various mechanisms of stress relaxation when the nanoparticle radius will increase. The same results are valid for pentagonal rods, which can be modeled by long elastic cylinders containing positive wedge disclinations along their axes.[2,19,29]

Howie and Marks[35] extended the disclination description to icosahedral nanoparticles (Fig. 12.2 (c)). They considered:

> an elastic sphere having the same missing volume (about 12%), but spread uniformly throughout the sphere. This is equivalent to an angular average of the strains, and may be visualized as a multitude of thin radial cones, each subtending a very small solid angle $d\omega$ at the centre, with small angular gaps between them in the unstrained state. The cones are now constrained by external forces to remain of the same length R while they are distorted sideways until they touch, are then 'glued' together. (Howie and Marks[35])

This process, which replaces the discrete set of six wedge disclinations each of strength $\omega \approx 7°21'$ by continuously distributed cone defects each of infinitely small strength $d\omega$, produces the distributed disclination which is now called Marks–Ioffe disclination.[36] The Marks–Ioffe disclination is characterized by the eigenstrain $\varepsilon^*_{\theta\theta} = \varepsilon^*_{\phi\phi} = 6\omega/4\pi \approx 0.0613$ and creates the elastic stresses:[35]

$$\sigma_{rr} = 4D\omega(1+\nu)\ln\frac{r}{R}, \quad \sigma_{\theta\theta} = \sigma_{\phi\phi} = 4D\omega(1+\nu)\left(\ln\frac{r}{R}+\frac{1}{2}\right), \qquad [12.4]$$

where (r, θ, ϕ) is the spherical coordinate system with the origin in the center of the sphere. Again the central region of the nanoparticle is compressed while its periphery is stretched. The hydrostatic stress $\sigma = 4/3D\omega(1+\nu)[3\ln(r/R)+1]$ is negative at $r < 0.7R$, zero at $r \approx 0.7R$ and positive at $r > 0.7R$. The stress components [12.4] are singular at $r = 0$. The strain energy is[35] $W_{Ic} = 4/3D\omega^2(1+\nu)R^3$.

Since the strain energy of the fivefold-twinned nanoparticles drastically increases with their radii, the nanoparticle structure is unstable with respect to various transformations. This may concern the surface faceting[37] and reconstruction,[38] structural modification and transition to 'normal' single crystalline state,[15,18–23] and formation of specific defect structures, which accommodate in part the initial strained state.[2,15,18–25,36] In particular, Gryaznov *et al*.[39] have theoretically considered the following relaxation channels of elastic stresses inside the pentagonal whiskers: 1) creating an edge dislocation inside the whisker, 2) opening a gap in the whisker, 3) creating a compensating negative partial wedge disclination near the whisker surface, 4) splitting the pentagonal axis (in terms of splitting the positive wedge disclination (Fig. 12.2 (a)) into a pair of similar disclinations of the same total strength), 5) growing a single crystalline (non-pentagonal) region in the whisker center, and 6) displacing the pentagonal axis from the whisker center. The authors calculated and compared the energy changes, which are characteristic for the relaxation channels, and concluded that the principal channels are dislocation creation, displacement and splitting of the pentagonal axis. Recently Kolesnikova and Romanov have analysed the formation of a circular prismatic dislocation loop in the cross section of a pentagonal whisker[40] and growth of a misfitting layer on the whisker surface[41] as potential channels of stress relaxation. The latter stress relaxation channel has also been applied to icosahedral nanoparticles.[36] For the case of an atomically heterogeneous pentagonal whisker, Panpurin and Gutkin[42] have studied the nucleation of a

precipitate in the shape of a finite-length cylinder coaxial to the whisker. In the approximation that the precipitate is subject of an axial positive eigenstrain ε^*, they have demonstrated that nucleation and growth of the precipitate are energetically preferable if ε^* is smaller than a critical value ε_c. If the eigenstrain is large ($\varepsilon^* < \varepsilon_c$, $\varepsilon^* \sim \varepsilon_c$) then the optimal shape of the precipitate is a thin disk, if small ($\varepsilon^* << \varepsilon_c$) then it is an elongated thin cylinder.

Concluding this section, it is worth noting that fivefold twinning has been observed not only in separate nanoparticles but also in their dense conglomerates obtained by inert gas condensation and compaction[43] and by severe plastic deformation.[44–47] Recent theoretical scheme[48] and computer simulations[49–51] have demonstrated that fivefold twins can be formed by a subsequent glide of Shockley partial dislocations in a nanocrystalline FCC material under extremely high local shear stresses.

12.2.2 Grain boundary sources of elastic strains

When nanoparticles compose dense conglomerates, i. e. nanocrystalline solids, the principal sources of elastic strains are defects associated with grain boundaries (GBs). It is also the case with GBs in coarse-grained polycrystalline materials, where the approach of periodic dislocation networks can be applied.[52] As was shown by many authors, in NCMs, the GBs are naturally short, often wavy, stepped and curved, and contain various extrinsic defects,[3,10,53–62] especially when the NCMs are produced by one of the methods of severe plastic deformation. These GBs are commonly called non-equilibrium GBs.[10] The most powerful GB defects are extrinsic GB dislocations,[63] GB and triple-junction disclinations.[64–67] All these defects are capable of creating long-range fields of elastic strains and stresses even in the absence of external loading. Such long-range elastic fields were registered in many experiments and attributed to various GB defects (see, for example,[10,59,61,68–73]).

Since the ensemble of GB defects in NCMs is rather irregular, their theoretical description within the periodic approach[52] would be incorrect. In the framework of analytical continuum modeling, which is the subject of the present review, two main alternative approaches can be considered. The first one was suggested by Nazarov *et al*.[74–77] who introduced some elements of disorder in modeling two-dimensional square networks of non-equilibrium GBs. The non-equilibrium GBs were modeled as GBs containing some typical self-screened configurations (edge dislocation dipoles and wedge disclination quadrupoles) of extrinsic GB dislocations[75,76] and GB junction disclinations.[76,77] The extrinsic GB dislocations were disordered due to the random distribution of slip lines in grains. The disorder was approximated by the uniform–random distribution, 'which means that the probability function of dislocation positions is uniform along GBs'.[76] The disorder of the GB junction disclination ensemble, which appears due to incompatibilities of the plastic deformation of neighbouring grains, concerned their strengths:

> Due to the random orientation of grains, the strengths of disclinations are also random variables. However, they are not completely independent. Indeed, a slip in each grain tends to form a disclination quadrupole with a strength ω_{ij} depending on the strain of the grain. Quadrupole strengths ω_{ij} are random variables, which can be considered as independent. The mean value of ω_{ij} is equal to zero. Then, the strength Ω_{ij} of a junction disclination is the sum of strengths of four disclinations[76] . . .

appearing at the junction of four neighbouring grains. Within such a model, Nazarov *et al*.[76] estimated the root mean square elastic strain ε_i, excess GB energy γ_{ex} and volume expansion $\Delta V/V$ of a NCM. For nc-Ni_3Al with the grain size d = 50 nm, the contribution of extrinsic GB dislocations was calculated as $\varepsilon_i \approx 5.8 \cdot 10^{-3}$, which is in the range of experimental data $\varepsilon_i \approx (5. . .10) \cdot 10^{-3}$.[68] The disclination contribution was estimated by $\varepsilon_i \approx 3 \cdot 10^{-3}$. For γ_{ex} and $\Delta V/V$ in Al with d = 100 nm, the dislocation and disclination contributions were estimated as $\gamma_{ex} \approx 0.3$ and 0.06 J m^{-2}, and $\Delta V/V \approx 4 \cdot 10^{-4}$ and $\Delta V/V \approx 0.08 \cdot 10^{-4}$, respectively.[76] Thus, it was shown that the dislocation contributions prevail over the disclination contributions in the NCMs under discussion. Later examples for some other NCMs showed the same proportions.[77] It is worth noting, that application of this approach is limited by the case of relatively coarse-grained NCMs with rather large grain size d ($\geq$ 50 nm) obtained by severe plastic deformation, because in relatively fine-grained NCMs with $d < 50$ nm, some of the assumptions used (for example, about intragranular slip, high density of extrinsic GB dislocations and GB junction disclinations, etc.) stop working.

Within the second approach, they consider a representative element of the GB defect structure and neglect the effect of similar neighbouring elements, thus suggested a weak elastic interaction between them. This approach allows one to describe in detail the elastically strained state in vicinity of the chosen element and is especially effective for modeling the initial stages of plastic deformation and fracture in 'weak sites' of NCMs. Earlier theoretical works of this direction have been discussed in monograph,[78] while some recent models and results are the subject of Section 12.3 of the present chapter.

12.2.3 Grain boundary stress concentrators

Apart from various defects, which create their proper elastic fields even in the absence of external loading (see Section 12.2.2), GBs in NCMs often contain defects which serve as stress concentrators under external load, such as pile-ups of GB dislocations, second-phase particles, nanocracks and nanopores. Pile-ups of GB dislocations can be formed in the process of GB sliding, which occurs via the motion of mobile GB dislocations with the Burgers vectors parallel to the GB planes. Triple junctions of GBs are effective obstacles for the gliding GB dislocations and, therefore, act as the places where pile-ups form under an applied

shear stress. At certain conditions, GB sliding can dominate over other mechanisms of plastic deformation in NCMs,[72,78–82] in which case one can expect massive formation and subsequent transformation[78] of GB dislocation pile-ups. As follows from the classical dislocation theory,[83] the stress concentration in the head of a dislocation pile-up is in direct proportion with the number of the pile-up dislocations. Therefore, the GB triple junctions, where the GB dislocation pile-ups form, must be subject to very high shear stresses and serve as places of further plastic relaxation[72,78,80,82] or crack nucleation.[84–86]

In pure NCMs produced by severe plastic deformation, second-phase particles often form from a small amount of substitutional solutes, which are always present in the material and surrounding atmosphere.[59,87] These ultrafine particles are located along GBs and their junctions, create their proper misfit strains and also serve as concentrators of external stresses. For example, the extended TEM studies of Kozlov *et al*.[87] and Koneva[59] have revealed the presence of $Cu_3Sn(Sb)$, Cu_3N, Cu_3O and CuO nanoparticles in ultrafine-grained Cu, and of Ni_4N, NiO and Ni_2O_3 nanoparticles in ultrafine-grained Ni. Elastic fields of these nanoparticles have also been demonstrated.

The role of pores and cracks as external stress concentrators is well known. Their presence in as-prepared and plastically deformed NCMs is also well documented.[3,43,84,88–91] This especially concerns the inert gas condensed NCMs, where the porosity is always rather high. The capacity of pores and cracks to concentrate external stresses has been used in a number of theoretical models describing the activation of various mechanisms of plastic deformation in NCMs.[92–96]

12.3 Plastic deformation in nanocrystalline metals

In recent years, the principal features and mechanisms of plastic deformation in NCMs have been comprehensively described in a number of reviews[10,97–130] and books.[78,131–133] Here we give some general remarks and briefly consider some recent theoretical models illustrating a large variety of deformation processes in NCMs.

Depending on the grain size d and test conditions, the following basic mechanisms of plastic deformation can be realized in NCMs (Fig. 12.3): (a) slip of lattice dislocations, (b) slip of GB dislocations, (c) mass transfer along GBs (Coble creep), (d) mass transfer along GB triple junctions, (e) migration of GBs, (f) deformation twinning, and (g) rotation of grains. Some of these mechanisms can compete with each other. Due to the grain distribution in size, different mechanisms of plasticity can dominate in different grains. In relatively large grains ($d > 20$–30 nm), the lattice dislocation slip usually dominates over the other mechanisms, while in relatively small grains ($d < 20$ nm), GB mediated mechanisms of plasticity dominate. In the next subsection we consider some theoretical models of dislocation nucleation in nanograins.

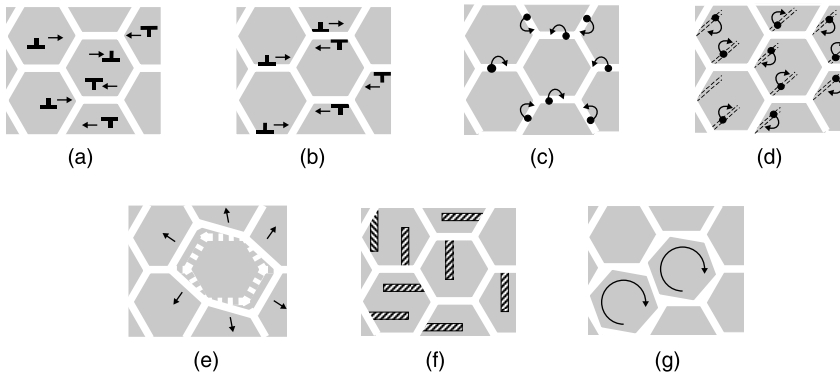

12.3 Schematics of mechanisms of plastic deformation acting in nanocrystalline metals: (a) slip of lattice dislocations, (b) slip of grain boundary dislocations, (c) mass transfer along grain boundaries (Coble creep), (d) mass transfer along triple junctions, (e) migration of grain boundaries, (c) deformation twinning, and (g) rotation of grains.

12.3.1 Mechanisms of dislocation generation

It is well known that the action of standard dislocation sources (like Frank–Read ones) is suppressed in NCMs, and GBs serve as the principal sources of lattice dislocations. However, some additional mechanisms of dislocation nucleation can also be activated under very high elastic stresses typical for NCMs under deformation. One of such possible mechanisms is the non-local homogeneous nucleation of nanoscale loops of 'non-crystallographic' partial dislocation, whose Burgers vector magnitude continuously grows during the nucleation process.[134,135] In contrast with the standard mechanism of local homogeneous nucleation of a perfect or partial lattice dislocation with fixed Burgers vector $\boldsymbol{B}$ (Figs. 12.4 (a)–(d)), which is characterized by a high-energy barrier,[83,136] this 'special' mechanism represents the nucleation of a finite glide dislocation loop of size L with variable strength $\boldsymbol{s}$ (Figs. 12.4 (a), 12.4 (e)–(g)). The latter model was motivated by experimental HREM observations of similar nonstandard atomic configurations called 'nanodisturbances' in Gum Metal,[137] which are capable of reversibly transforming to dipoles of lattice dislocations under an applied stress.[138]

Homogeneous nucleation of a glide loop of 'non-crystallographic' partial dislocation (Figs. 12.4 (a), 12.4 (e)–(g)) in an infinite elastically isotropic solid under the action of an external shear stress τ is accompanied by a change ΔW in the total energy of the system. For the loop having a shape of a planar square of size L and characterized by the Burgers vector $\boldsymbol{s}$, whose magnitude lies within the interval $0 < s \leq B$, the energy change can be approximated by equation:[135]

$$\Delta W = Db^3 \left\{ x^2 y(2-\nu)\left(\ln\frac{y}{x} + 1.22 \right) + (y-2x)^2 \frac{\gamma(x)}{Db} - xy^2 \frac{\tau}{D} \right\}, \quad [12.5]$$

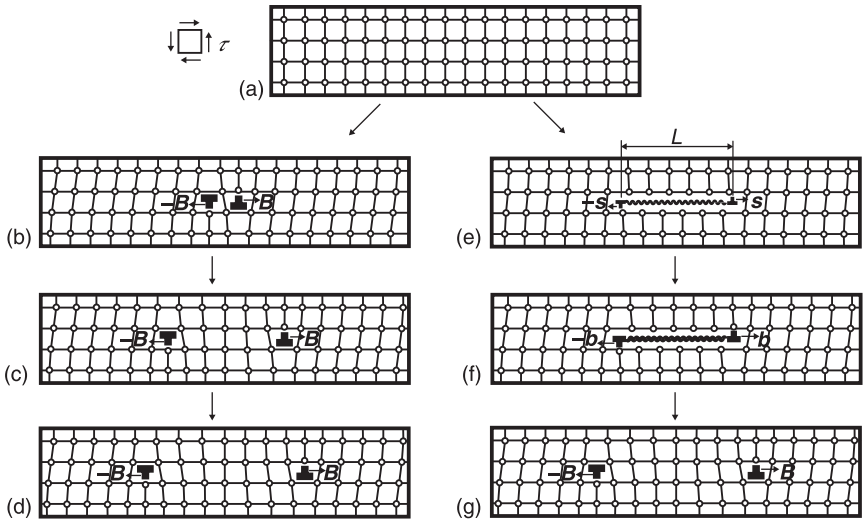

12.4 Two-dimensional representation of crystal lattice transformations corresponding to (a)–(d) standard homogeneous generation and extension of a gliding square loop of perfect lattice dislocation with Burgers vector $\boldsymbol{B}$, and (e)–(g) non-local homogeneous generation of a gliding square loop of 'non-crystallographic' partial dislocation with a finite size L and small Burgers vector $\boldsymbol{s}$ ($0 < s \le B$) under an external shear stress τ. When s increases and achieves the magnitude b, the latter loop is transformed into a 'normal' loop of partial lattice dislocation with Burgers vector $\boldsymbol{b}$; with further increase of s, it transforms into a 'normal' loop of perfect lattice dislocation with Burgers vector $\boldsymbol{B} \approx 2\boldsymbol{b}$.[135]

where $D = G/[2\pi(1-\nu)]$, G is the shear modulus, ν is the Poisson ratio, $b \approx B/2$ is the magnitude of a partial lattice dislocation, $x = s/b$ and $y = L/b$ are the dimensionless parameters, and $\gamma(x)$ is the specific (per unit area) energy of a generalized stacking fault approximated as follows:[135]

$$\gamma(s) = \begin{cases} \gamma_m \sin\dfrac{2\pi s}{B}, & \text{if} \quad s < \dfrac{B}{4} \\ \dfrac{\gamma_m + \gamma_0}{2} - \dfrac{\gamma_m - \gamma_0}{2}\cos\dfrac{4\pi s}{B}, & \text{if} \quad \dfrac{B}{4} \le s < \dfrac{3B}{4}. \\ -\gamma_m \sin\dfrac{2\pi s}{B}, & \text{if} \quad \dfrac{3B}{4} \le s \le B \end{cases} \qquad [12.6]$$

The system of equation [12.6] describes a 'two-humped' dependence, which has its minimum corresponding to the specific energy γ_0 of a conventional stable stacking fault, and two maximums corresponding to the energy γ_m of two unstable stacking faults. Similar 'two-humped' dependences of the energy γ on the shear s,

which characterize generalized stacking faults in various solids, were obtained in many computer simulations.[139–143]

The function $\Delta W(x, y)$ was analysed for two typical NCMs, Al and Ni, with the following values of the model parameters: for Al,[83,141] $G = 27$ GPa, $\nu = 0.31$, $b \approx 0.143$ nm, $\gamma_0 = 99$ mJ/m^2 and $\gamma_m = 164$ mJ/m^2; for Ni,[83,142] $G = 73$ GPa, $\nu = 0.34$, $b \approx 0.125$ nm, $\gamma_0 \approx 120$ mJ/m^2 and $\gamma_m \approx 170$ mJ/m^2. With equations [12.5] and [12.6], the maps for the energy change function $\Delta W(x, y)$ were calculated.[135] Three of these maps for Al at various magnitudes of the applied shear stress τ are shown in Fig. 12.5. For Ni, the energy maps are similar in their general features. In both the cases, Al and Ni, when τ is relatively small, there are two characteristic energy barriers along the axes $x = s/b$ and $y = L/b$ (Fig. 12.5 (a)). These barriers must be overcome in order to nucleate a dislocation loop. For Al, the saddle point $\Delta W_s(\tau = 2\text{GPa}) \approx 4.55$ eV has approximate coordinates ($s/b \approx 0.83$, $L/b \approx 22$). For Ni, the saddle point $\Delta W_s(\tau = 3\text{GPa}) \approx 19.05$ eV is located approximately at ($s/b \approx 0.72$, $L/b \approx 48$). These values of ΔW_s are high, and the loop can hardly nucleate.

If τ is large enough ($\tau \geq 3.7$ GPa for Al and $\tau \geq 4.4$ GPa for Ni), the situation drastically changes (Fig. 12.5 (b), 12.5 (c)). The 'left' energy barriers disappear and a dislocation loop can nucleate through increase of its strength s and size L without any barrier. The thick arrowed curves approximately show the barrier-less evolution of a dislocation loop in the (s/b, L/b) space or, in other terms, the (x, y) space. Let us consider in detail stages of barrier-less evolution shown in Fig. 12.5 (b), (c). When τ is comparatively small (Fig. 12.5 (b)), the dislocation loop first grows mainly in size. The dislocation strength s is rather low ($s \leq b/20$) at this stage. When the dislocation loop parameters, s and L, achieve the first critical region ($x \approx x_{c1}$, $y \approx y_{c1}$) in the map of $\Delta W(x, y)$, the loop stops extending and starts to grow in strength. The point (x_{c1}, y_{c1}) corresponds to disappearance of 'left' minima at the contours $y(x)$. As a result, the loop of fixed size increases in strength and finally transforms into a loop of perfect lattice dislocation. When τ is comparatively large (Fig. 12.5 (c)), the loop first grows in both size and strength (here $s \leq b/10$) and also attains the first critical region. After this event, the dislocation loop increases in strength until $x \approx 1$, corresponding to the Burgers vector of a partial lattice dislocation. This area of the map may be considered as the second critical region ($x \approx x_{c2}$, $y \approx y_{c2}$), where the 'right' minima at the contours $y(x)$ appear. Between the above second critical region and the third critical region ($x \approx x_{c3}$, $y \approx y_{c3}$), where the 'right' minima at the contours $y(x)$ disappear, evolution of the dislocation loop parameters occurs through growth of both the size and strength of the loop. When the loop parameters, s and L, cross the third critical region, the dislocation loop again practically stops extending and only increases in strength until it reaches the Burgers vector of perfect lattice dislocation.

Thus, the special mechanism of homogeneous nucleation[135] can effectively operate in a barrier-less way and produce loops of partial and perfect lattice dislocations in NCMs (Al, Ni) deformed at high mechanical stresses. This level of external stress can be achieved in shock-wave and indentation load regimes.

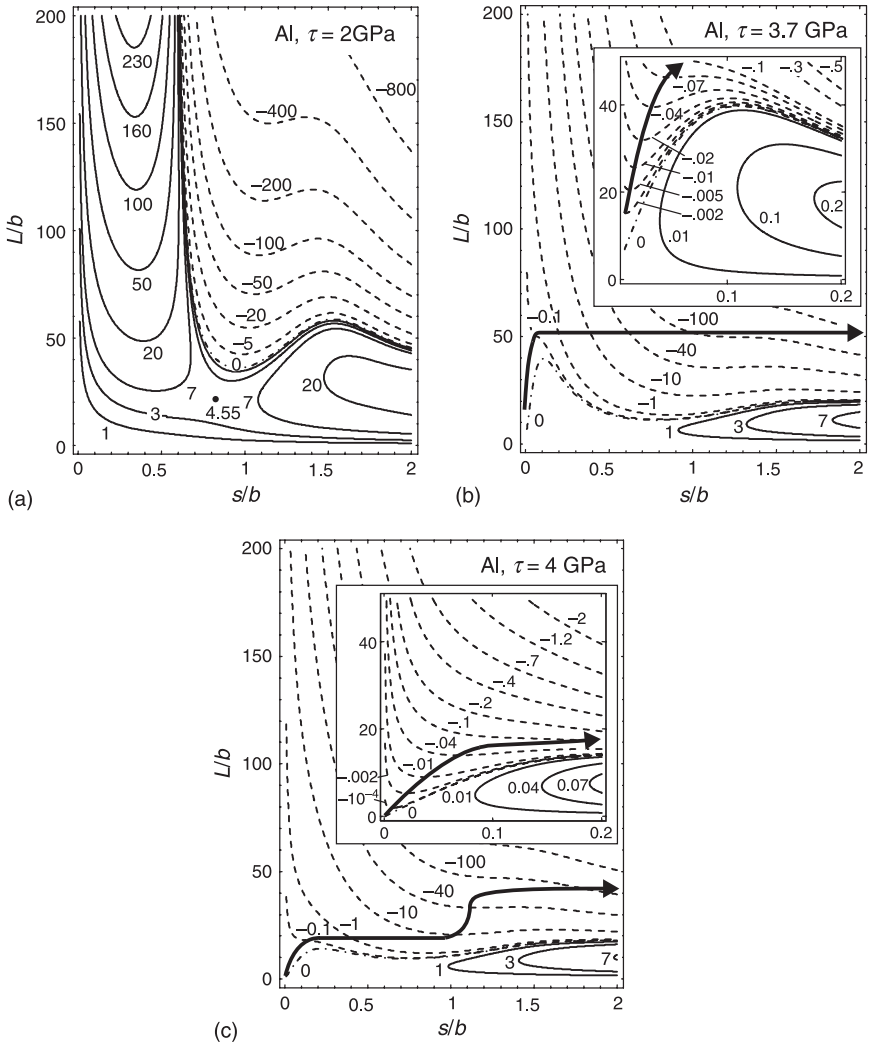

12.5 Maps of the energy change $\Delta W(x, y)$, where $x = s/b$ and $y = L/b$, for pure Al under the external shear stress (a) $\tau = 2$ GPa, (b) 3.7 GPa, and (c) 4 GPa. The values of ΔW are given in eV. The bold dot in map (a) shows the saddle point. The thick arrowed curves in maps (b, c) approximately image the barrier-less evolution of a dislocation loop in strength and size. The insets in plots (b, c) show the enlarged maps for small s and L.

Besides, with the existence of numerous stress sources and concentrators in NCMs (see Section 12.2), local stresses can reach very high values and thereby cause the homogeneous nucleation of dislocation loops in these materials at even quasistatic load regimes. Recently, ultrahigh strain rate ($>10^7$ s^{-1}) and pressures

(20–70 GPa) have been achieved in experiments[144] on laser-driven compression of nc-Ni with grain sizes of 30–100 nm. Postmortem TEM characterization revealed that the nanocrystalline structures survived the shock load and that the dislocation slip mechanism is essential or even dominant. In particular, the dislocation density was estimated to be around 10^{16} m^{-2} in a nc-Ni sample after compression at 40 GPa pressure on nanosecond timescales. The origin of this remarkably high dislocation density has been not identified. In the context of the theoretical results,[135] the non-local homogeneous nucleation of dislocation loops appears likely to be responsible for a generation of high-density dislocation ensembles in nanocrystalline Ni (and, probably, other NCMs) under shock-wave deformation.

Among the most important issues for the mechanical behavior of NCMs is their ability to suppress plastic flow localization in shear bands.[145–147] This has generated interest in identifying the role of GBs and their transformations in the formation and evolution of shear bands in NCMs. In ductile NCMs with comparatively large grains with size $d \geq 30$ nm, where the lattice dislocation slip is still dominant, GBs can serve as effective sources of perfect and partial lattice dislocations. In earlier theoretical models[148–150] of emission of perfect lattice dislocations by high-angle GBs in fine-grained materials, the emission intensity was assumed to be controlled by movement and transformations of GB dislocations[148] and disclinations.[149,150] These processes are too slow to cause the formation of high-density ensembles of mobile lattice dislocations that would carry large plastic strains in shear bands. At the same time, NCMs contain low-angle GBs consisting of lattice dislocations.[151] Such low-angle GBs undergo structural transformations under internal stresses in coarse-grained polycrystalline materials.[63] It seems natural to expect the same in mechanically loaded NCMs, too. Below we briefly discuss some theoretical models of GB transformations under external loading.

Following Bobylev *et al.*,[152–154] consider a model low-angle tilt boundary terminated at triple junctions of GBs in a nanocrystalline sample (Fig. 12.6 (a)).

The low-angle boundary in its initial state (in the absence of mechanical load) is represented as a straight wall of periodically arranged edge dislocations with Burgers vector $\boldsymbol{b}$ and characterized by the misorientation angle θ being in the Frank relationship, $\sin(\theta/2) = b/(2h)$,[63] with the period h and the Burgers vector magnitude b. Also, for definiteness, the angle θ is assumed to be in compensating relations, $\theta+\theta_1+\theta_2 = 0$ and $-\theta+\theta'_1+\theta'_2 = 0$, with the tilt misorientation parameters, (θ_1, θ_2) and (θ'_1, θ'_2), of the GBs adjacent to the upper and bottom triple junctions, respectively. In other words, the upper and bottom edges of the finite dislocation wall in its initial state (Fig. 12.6 (a)) completely compensate for the disclination defects A and B (shown as triangles) at the upper and bottom junctions of the adjacent GBs, respectively. The action of a shear stress τ on the edge dislocations, composing the low-angle GB, causes their displacements from the initial positions (Fig. 12.6 (b)). At a critical value $\tau = \tau_c$, one of the dislocations releases and starts

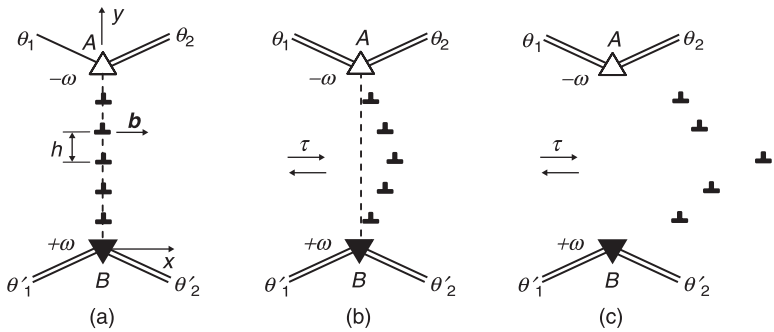

12.6 Decay of a low-angle tilt boundary represented as a dislocation wall *AB*: (a) initial state of the wall, (b) bowing of the wall, and (c) decay of the wall.

moving far from the initial GB plane. This is immediately followed by decay of the dislocation wall as a whole (Fig. 12.6 (c)). As a result, a group of lattice dislocations released from the decayed low-angle GB move, causing local plastic deformation and the formation of an elongated grain. Following experimental data,[145,155] such elongated grains are characteristic structural elements of shear bands in nanocrystalline Fe. A similar process of decay of a low-angle boundary has been observed in molecular dynamics simulations of plastic deformation in nc-Ni,[156] Al[157] and Pd.[158]

The wall decay transforms the GB triple junctions into uncompensated double junctions *A* and *B* (Fig. 12.6 (c)). They become stress sources of disclination type, characterized by strength $\pm\omega = \pm\theta$. The stress field of the disclination dipole *AB* causes a hampering force on the moving lattice dislocations after the decay of the GB. The critical shear stress τ_c was calculated within 2D dislocation dynamics.[152–154] As an example, the decay of a GB composed of $N = 15$ dislocations and characterized by angle $\theta = 0.1$ (≈5.7°) in nanocrystalline Fe was studied in detail.[153] It was found that at $\tau \leq 1.53$ GPa, the dislocations made some oscillations and were finally stabilized at some equilibrium positions, which were shifted further with increasing τ (see curves 1 to 5 in Fig. 12.7 (a)). When $\tau > \tau_c$ (here $\tau_c = 1.53$ GPa), the central dislocation moved far away from its initial position (see curve 6 in Fig. 12.7 (a)), and the GB decayed as a whole. The analysis of stability of low-angle GBs with different parameters showed that τ_c grows in a roughly linear way with rising θ (see curve 1 in Fig. 12.7 (b)). On the other hand, the dependence of τ_c on the number N of dislocations, and thereby the GB length d (= Nh) at a constant value of θ, is very weak. This means that very short GBs in very small grains and comparatively long GBs in large grains decay at close values of the critical stress τ_c, if they have the same misorientation θ.

The decay of a low-angle GB results in the formation of moving lattice dislocations that elastically interact with other lattice dislocations composing

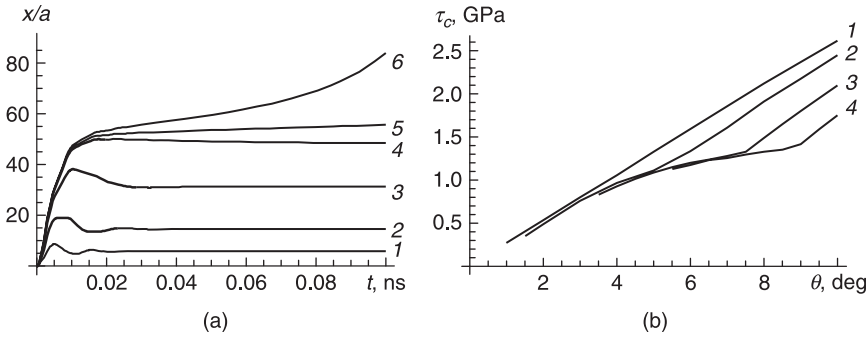

12.7 (a) Temporal dependence of the position x of the 8th dislocation in a low-angle GB with $\theta = 0.1$ and $N = 15$, for $\tau = 0.5$, 1.0, 1.4, 1.52, 1.53 and 1.54 GPa (curves 1, 2, 3, 4, 5 and 6, respectively). (b) Dependences $\tau_c(\theta)$ for $\omega_l = 0°$, 1°, 3°, and 5° (curves 1, 2, 3, and 4, respectively).

neighbouring low-angle GBs. This interaction is able to stimulate decays of the neighbouring low-angle GBs and avalanche-like release of new mobile lattice dislocations.[153,154] The main results are demonstrated in Fig. 12.7 (b), where the curves $\tau_c(\theta)$ are plotted for different values of the strength ω_l characterizing a disclination dipole that has been formed after the decay of a neighbouring low-angle GB. As was expected, the critical shear stress τ_c decreases with rising ω_l. The phenomenon in question is able of causing plastic flow localization (carried by lattice dislocations released by low-angle GBs) in deformed NCMs containing high-density ensembles of low-angle GBs.

As shown experimentally, high-angle GBs bow (become curved)[84,159] and emit partial lattice dislocations[47,159–164] that can provide deformation twinning in NCMs. To account for these experiments, Bobylev *et al.*[153] extended the above model to the case of high-angle GBs containing GB dislocations. In general, high-angle GBs contain intrinsic dislocations with small Burgers vectors associated with misorientation of such GBs. They cannot glide easily in the grain interior, in contrast to the lattice dislocations. However, high-angle GBs bow and emit partial dislocations into adjacent grains in mechanically loaded NCMs (Fig. 12.8).

Bobylev *et al.*[153] first considered the GB bowing under a shear stress τ by means of 2D dislocation dynamics that account for the additional hampering force due to an increase of the GB length. Solution of the system of dynamics equations, adapted to this case, gives new equilibrium positions of the GB dislocations and, as a corollary, an equilibrium configuration of the high-angle GB in its curved state (Fig. 12.8 (b)). Now let one of the GB dislocations located at the curved GB split into an immobile GB dislocation and a mobile Shockley dislocation that moves in the adjacent grain interior under a stress τ (Fig. 12.8 (c)). The authors

calculated the energetics of the dislocation emission, which was considered as a transformation of the system from its initial state with the energy W_1 (Fig. 12.8 (b)) to the final state with the energy W_2 (Fig. 12.8 (c)). The dislocation emission is energetically favourable, if the energy difference $\Delta W = W_2 - W_1 - A$ is negative. Here A is the work spent to transfer the Shockley dislocation under the stress τ. The energy difference ΔW was analysed for the exemplary case of pure nanocrystalline Cu, when the GB is characterized by the deviation ω of the GB tilt misorientation θ from that, θ_0, of a low-energy (favourable) GB in the same material.[63] The favourable GB $\Sigma = 5/(210)$ with[165] misorientation angle $\theta_0 = 36.87°$ and specific energy $\gamma = 0.9$ J·m^{-2} was used. It was shown that an increase in τ enhances the splitting and emission processes (Fig. 12.9 (a)). At the same time, the dislocation emission is energetically unfavourable at low τ and is hampered with rising ω (Fig. 12.9 (b)).

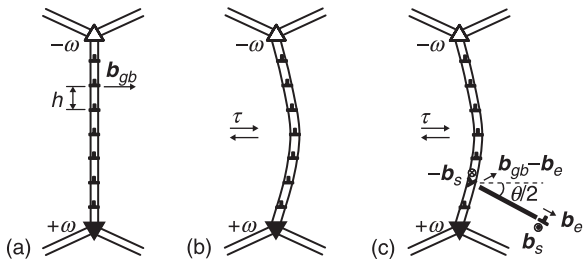

12.8 Evolution of a high-angle GB with intrisic GB dislocations: (a) initial state, (b) bowing of GB, and (c) splitting of a GB dislocation and emission of a partial Shockley dislocation. The partial dislocation has Burgers vector with the edge ($\boldsymbol{b}_e$) and screw ($\boldsymbol{b}_s$) components. Its glide causes a stacking fault. The immobile GB dislocation has the Burgers vector with the edge ($\boldsymbol{b}_{gb} - \boldsymbol{b}_e$) and screw ($-\boldsymbol{b}_s$) components.

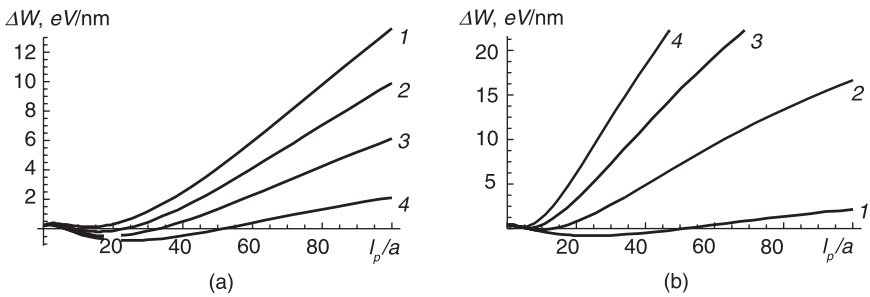

12.9 The energy change ΔW via the path l_p of the 5th partial dislocation in the case of high-angle GB containing $N = 20$ GB dislocations, for (a) $\omega = 3°$ and $\tau = 0.4$, 0.6, 0.8, and 1.0 GPa (curves 1, 2, 3 and 4, respectively); and (b) $\tau = 1$ GPa and $\omega = 3°$, 5°, 7°, and 9° (curves 1, 2, 3 and 4, respectively).

Let us discuss now the emission of partial dislocation by a GB disclination. Following Gutkin *et al.*,[166] consider a 2D model of a NCM with positive and negative wedge GB disclinations of a mean strength ω. Let such a disclination ensemble consist of disclination dipoles with a mean arm (grain size) d, which are distant by $2R$ from each other, and $d < R$ (Fig. 12.10 (a)).

In this case, one can analyse a separate GB disclination dipole as a source for generation of lattice dislocations (Fig. 12.10 (b)). Within an energy-based approach, we calculated some critical values of the external shear stress τ which correspond to the generation of a lattice dislocation, its localization in the bulk of the grain and its absorption by the opposite GB, depending on the principal parameters of the model: d, θ, and α (see Fig. 12.10 (b)). For example, in Fig. 12.11,[166] the curves $\tau_c(\theta)$ are shown which were calculated for the case of pure nanocrystalline Al at $\omega = 0.1$ ($\approx 6°$), $\alpha = 10°$ and $d = 10$, 20 and 30 nm. The curves $\tau_c(\theta)$ determine (if exist) those regions at the (θ,τ) diagram, where three typical arrangements of partial dislocations must appear in a grain: I, when partial dislocations are localized near their GB sources; II, when they are spread inside the grain; and III, when they cross the grain and are absorbed by the opposite GBs. An increase in the grain size d is accompanied with an extension of the

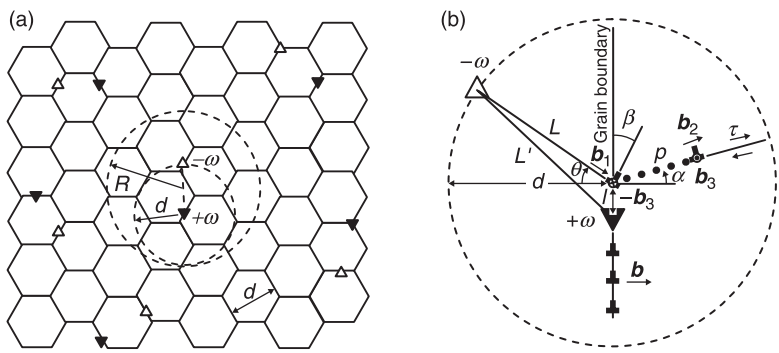

12.10 (a) 2D model of a NCM with positive and negative wedge GB disclinations. (b) Emission of a partial Shockley dislocation from a moving GB disclination. The positive GB disclination moves by a distance l ($l = b/[2\sin(\omega/2)]$ is the spacing between the intrisic GB dislocations with the Burgers vectors ($\boldsymbol{b}$), thus emitting a lattice dislocation. This dislocation may be either partial, with the Burgers vector having the edge ($\boldsymbol{b}_2$) and screw ($\boldsymbol{b}_3$) components, or perfect, with the Burgers vector $2\boldsymbol{b}_2$. At the place of generation, a difference GB dislocation forms, whose Burgers vector has either the edge ($\boldsymbol{b}_1 = \boldsymbol{b} - \boldsymbol{b}_2$) and screw ($-\boldsymbol{b}_3$) components, or only the edge component ($\boldsymbol{b} - 2\boldsymbol{b}_2$), respectively. The position of the negative GB disclination sets by the initial dipole arm $L \approx d$ and the azimuthal angle θ. The angle α determines the orientation of the dislocation gliding plane with respect to the GB.

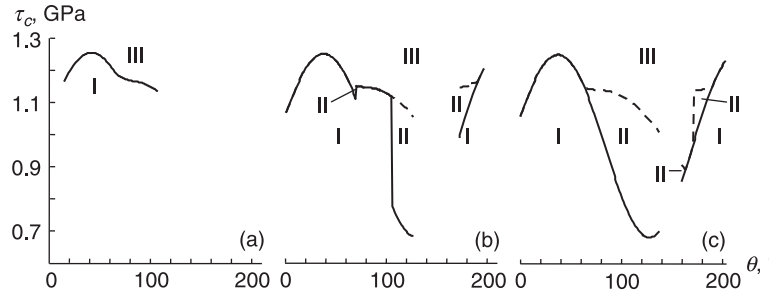

12.11 Critical stress τ_c via the azimuthal angle θ for different values of the grain size: (a) d = 10 nm, (b) d = 20 nm, and (c) d = 30 nm.

θ ranges, where the emission of partial dislocations must occur, and drastic changes in distribution of regions I, II and III (see Gutkin *et al*.[166] for details).

It is worth noting that these characteristic types of defect arrangements were observed in molecular dynamics simulations (for example, see[156,157]). As follows from calculations,[166] there exist two characteristic grain sizes in nanocrystalline Al: d_{c1} (≈ 5 nm) and d_{c2} (≈ 30 nm). When $d \le d_{c1}$, the generation of partial dislocations by GBs needs smaller values of τ than that of perfect dislocations, in the full range of possible values for θ and α. When $d \ge d_{c2}$, the generation of perfect dislocations becomes more energetically preferable for any of possible θ and α. In the grains of intermediate size, $d_{c1} < d < d_{c2}$, the generation of either partial or perfect dislocations may dominate, depending on the values of the angles θ and α.

Above we have considered some 2D models. However, the lattice dislocation slip, deformation twinning and GB sliding in real NCMs are 3D processes conducted by dislocation loops (DLs). In this context, a 3D description of the deformation mechanisms in terms of DLs seems to be important. As noted in Ref.[167] the effective way of interaction between different modes of plastic deformation in NCMs is the generation of new DLs at the pre–existent DLs of other types. For example, pre-existent grain boundary DLs (GBDLs) can serve as sources for perfect or partial lattice DLs (Fig. 12.12 (a), 12.12 (b)) or GBDLs (Fig. 12.12 (c)). The pre-existent perfect or partial lattice DL can generate either a perfect or partial lattice DL into the neighbouring grain (Fig. 12.12 (d)) or a GBDL (Fig. 12.12 (e)). To summarize, there are 9 variants of the DL generation at the pre-existent DLs, depending on the types (GB, perfect lattice, partial lattice) of these DLs. These variants are called the modes for the DL generation at pre-existent DLs. All these modes were analysed within a 3D energy-based approach for the exemplary case of nanocrystalline Al with the grain size d ranging from 10 to 100 nm.[167] The basic results are briefly as follows: 1) loops of perfect lattice dislocations operate as effective sources for GB, partial and perfect lattice DLs (in order of preference); 2) loops of partial lattice dislocations serve as

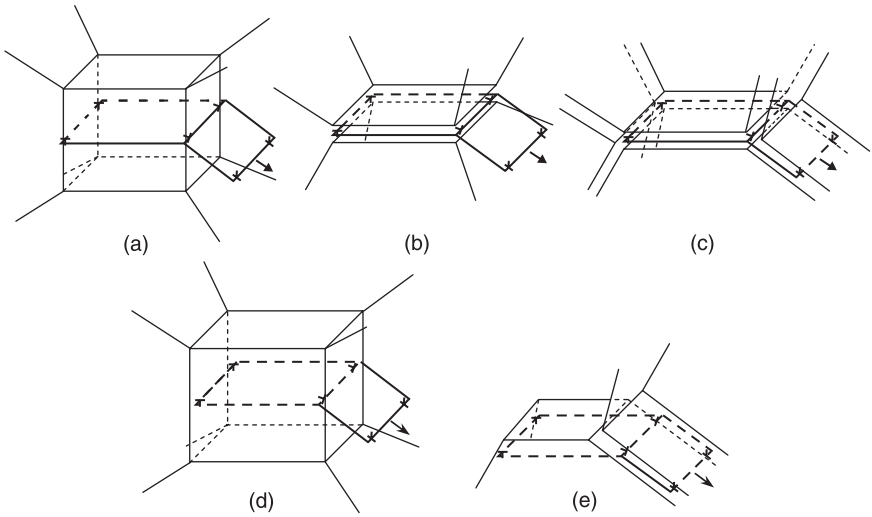

12.12 Different modes of generation of a new gliding DL at a segment of the initial gliding DL: (a,b) a lattice DL is emitted by a GBDL, (c) a GBDL is emitted by a GBDL, (d) a lattice DL is emitted by a lattice DL, (e) a GBDL is emitted by a lattice DL. In all the cases, a new DL is generated at a GB or at a triple junction of GBs.

effective sources for GB and partial lattice DLs (in order of preference), but are not effective to generate perfect lattice DLs; 3) loops of GB dislocations can be effective sources for GBDLs, while they are not so effective for generation of partial lattice DLs; GBDLs hardly can generate perfect lattice DLs. With these results, grains in NCMs can be divided into the three basic categories: relatively large ($d \approx 30$ to 100 nm), intermediate ($d \approx 10$ to 30 nm) and finest ($d \approx 3$ to 10 nm) grains. The lattice dislocation slip effectively operates in large grains. The most effective sources of new DLs here are loops of perfect lattice dislocations, in which case the lattice slip enhances intense GB sliding. In intermediate grains, the conventional lattice dislocation slip is severely suppressed. The most effective sources of new DLs here are loops of partial (twinning) lattice dislocations, which enhance GB sliding. In the finest grains, GB sliding dominates over the lattice dislocation slip and deformation twinning. Here GBDLs serve as effective sources of new GBDLs that cause intense GB sliding.

A further development of these 3D models was conducted by Bobylev *et al.*[168,169] with the aim to explain anomalously wide stacking faults (SFs) between partial dislocations in nanocrystalline Al. The theory of DLs was used to calculate the system energy more accurately compared to some earlier models.[105,170–173] By means of an original algorithm, the authors investigated both the generation of partial dislocation semi-loops and the dependence of the SF

width on the grain size and applied stress level. They showed that anomalously wide SFs in nanocrystalline Al are caused by high stresses but not by small grain size as was derived in the earlier models. On the other hand, it was noted[168] that 'such high stresses are possible in nanocrystalline Al because the normal dislocation activity is suppressed by the small grain size. Therefore, although the small grain size is not directly connected with anomalously wide SFs in nanocrystalline Al, it represents the primary cause of this phenomenon.'

12.3.2 Generation of deformation twins

As is well known, deformation twins (DTs) do not appear in coarse-grained metals with relatively high values of SF energy γ. A typical example is Al. The situation dramatically changes in the case of nanograins. DTs in nanocrystalline Al were observed in electron microscopy experiments.[159–161] To explain this phenomenon, a number of theoretical models[94,105,168–179] have recently been suggested that describe anomalously wide SFs whose overlapping would create DTs in nc-Al. However, some of these models[105,168–174,179] deal with only one or two SF strips and cannot directly be used in a description of the generation of thick DT lamellae observed experimentally in nc-Al,[160,161] Cu,[47,180,181] Ni,[84,182–187] Pd[188] and Ta.[189] Following the experiment, the DT lamellae have typical thickness of several nanometers and occupy regions between opposite GBs in nanograins. Sometimes DT lamellae form V-, T- and X-shaped configurations studied in detail by Zhu *et al*.[190]

Let us briefly consider some models that describe the generation of thick DT lamella at GBs in NCMs. It seems rather evident that probability of DT nucleation increases in vicinity of stress sources and concentrators. Extrinsic GB dislocations can stimulate the emission of Shockley partials (see Section 12.3.1); however, their density is not so high and their stresses are not strong enough for initiation of thick DT lamella nucleation.[176] Possible alternatives are GB disclinations[176,177] and cracks,[94] which create strong and long-range stress fields. In the model,[176] a DT lamella is nucleated under the action of an applied stress and the stress field of a dipole of GB or junction wedge disclinations (Fig. 12.13 (a)).

The model[176] was used to consider pure nanocrystalline Al and Cu with $d \approx$ 30 nm. It was shown that, if the disclination strength ω and external shear stress τ are high enough (but still realistic for these NCMs), the DT generation is characterized by the absence of any energy barrier. The critical stress τ_c causing the emission of the first twinning dislocation is rather low (≈0.1 GPa and ≈0.3 GPa, for Cu and Al, respectively, at $\omega = 0.5$). As the DT thickness (equal to $\delta(n-1)$, where δ is the distance between neighbouring {111} atomic planes and n is the number of emitted Shockley partials) increases, the critical stress $\tau_c(n)$ of the emission of new twinning dislocations first grows, then levels off, and again grows (Fig. 12.13 (b)). Thus, there are two stages of local hardening and an

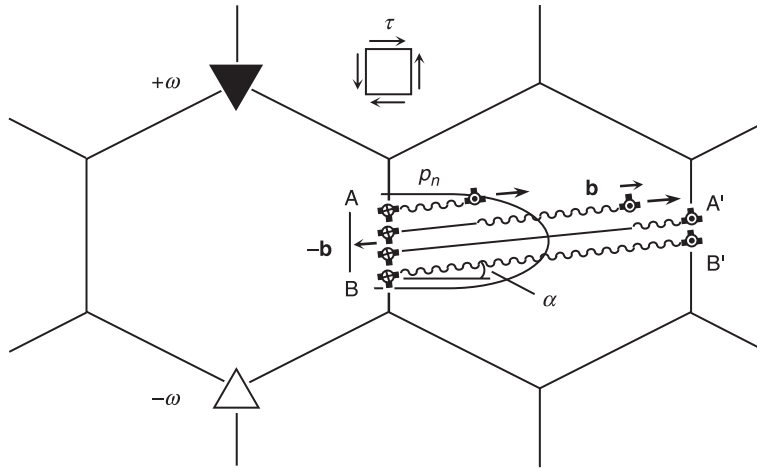

(a)

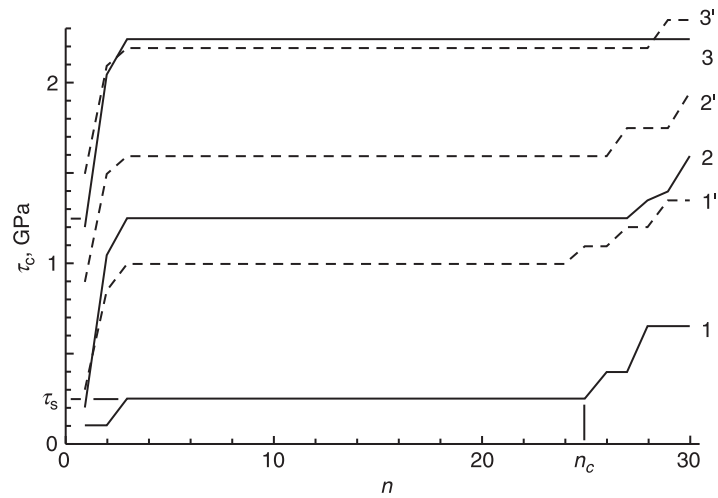

(b)

12.13 (a) The twinning partial dislocations are emitted from a GB segment AB in nanocrystalline sample with GB disclinations of strength $\pm\omega$. The emission occurred in the region (bounded by dashed contour) where the shear stress of the disclination dipole reaches its highest level. The combined action of the external shear stress τ and the disclination stress field causes the emission and glide of partials along the adjacent slip planes. Most of the partials reach the opposite GB at its segment A'B'. The overlapping stacking faults (generated behind the emitted partials) form the deformation twin lamella AA'B'B. (b) Dependence of the critical external shear stress τ_c on the number n of emitted partials in nanocrystalline Cu (solid curves) and Al (dashed curves), for disclination strength $\omega = 0.5$ (curves 1, 1'), 0.4 (2, 2'), and 0.3 (3, 3').

intermediate stage of local flow of a NCM on a scale of one nanograin. In all stages, τ_c depends strongly on ω; indeed, a decrease in ω results in a sharp increase in τ_c. When studying the dependence of the equilibrium position p_{eq} of a twinning dislocation on its ordinal number n, we found the shape of the DT front (Fig. 12.14).[177] Depending on the orientation of the disclination-dipole arm, the longitudinal section of DT lamella is close to a rectangle or a blunted wedge, which agrees well with the results of aforementioned experimental observations. The estimated DT thicknesses (5.6–7.0 nm for Al and 5–6 nm for Cu)[177] are also consistent with the experimental data.[47,160,161]

The model of DT lamella nucleation at an extrinsic GB dislocation aside of a crack tip (Fig. 12.15 (a)) has given similar results.[94] It was shown that, if the external shear stress τ and the crack length L are sufficiently large, no energy barrier exists for the nucleation of a DT. Such values of τ and L fall in the ranges typical of the NCMs under study. For example, in nc-Al with $d \approx 30$ nm the critical stress τ_c required for the nucleation of the first twinning dislocation at $L = 20d = 600$ nm is approximately 0.25 GPa (Fig. 12.15 (b)). For a micro-crack with $L = 200d = 6$ μm, the critical stress decreases to approximately 15 MPa. With

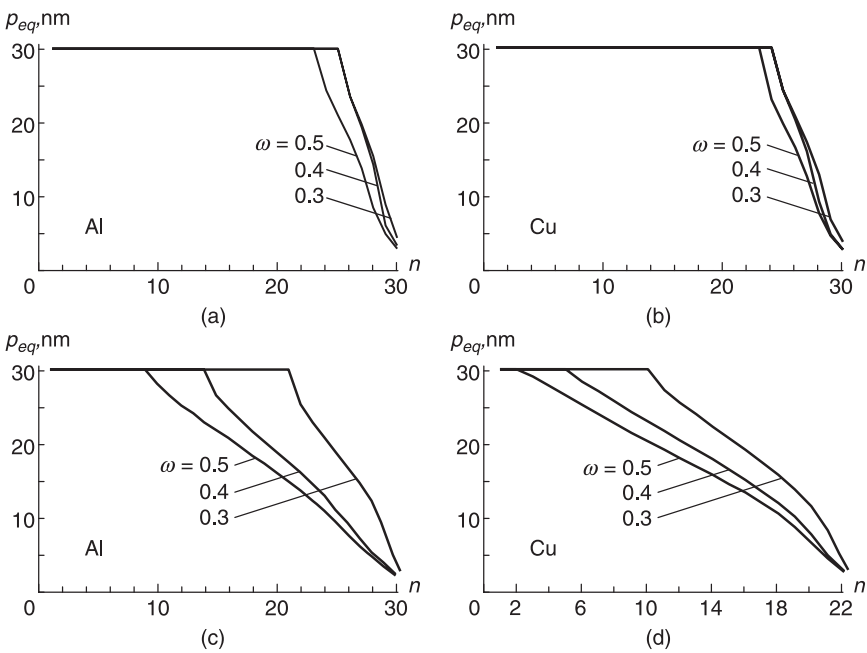

12.14 Dependence of the equilibrium position p_{eq} of a twinning dislocation on its ordinal number n in nanocrystalline (a, c) Al and (b, d) Cu for the disclination-dipole strength ω equal to 0.3, 0.4, and 0.5. The dipole arm is oriented (a, b) along or (c, d) normal to the grain boundary.

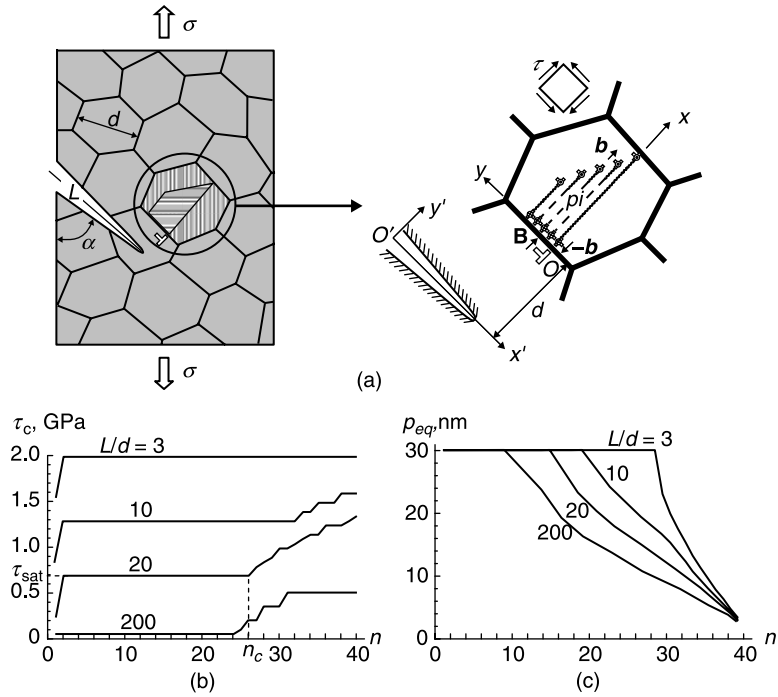

12.15 (a) Generation of a deformation-twin lamella at an extrinsic grain-boundary edge dislocation in the vicinity of a mixed I and II mode crack of length *L*. (b)–(c) The critical external shear stress τ_c and the equilibrium position p_{eq} of a twinning dislocation via its ordinal number *n* in nc–Al, for various values of the normalized crack length: L/d = 3, 10, 20 and 200.

raising the DT thickness, the critical stress of the emission of new twinning dislocations first grows, then saturates, and again grows, as is the case with DT generation in the disclination stress field.[176,177] In all the stages, the critical stress τ_c strongly depends on the crack length *L*. A decrease in *L* results in an increase in τ_c. The curves $p_{eq}(n)$, which determine the shape of the DT lamella, also depend on *L* (Fig. 12.15 (c)). Depending on *L*, the longitudinal section of DT lamella is close to a rectangle or a trapezoid. The DT thickness was found to vary from 3.5 to 9.4 nm in nc-Al. The lower (higher) limit corresponds to the maximum (minimum) length *L* of the crack under discussion and the minimum (maximum) value of the applied critical stress τ_c. The main conclusion is that microcracks can stimulate the nucleation of thick DT lamellae far from the crack tip. Recently Fischer *et al*.[178] have developed a similar micromechanical model and come to the same conclusion.

12.3.3 Rotational deformation

The principal structural features of NCMs, such as nanoscale grains, high volume fraction of grain boundaries and their triple junctions, and a high density of GB defects (see Section 12.2.2), provide many opportunities for development of rotational plastic deformation.[78,132] Rotational modes of plasticity include stress- and strain-driven formation of misorientation bands and new boundaries, change in GB misorientation angles and grain rotation, which are the processes of local reorientation of crystalline lattice.[66,78,132,191] These processes are realized through the collective behavior of lattice and/or GB dislocations that is effectively described in terms of partial disclinations.[27,29,64–67,78,102,132,191–193]

Experimental evidence of rotational plasticity in deformed NCMs has been demonstrated in many works.[194–205] Recent direct HRTEM observations of Murayama *et al*.[195] have approved the existence of partial wedge disclinations in severely deformed nc-Fe. Ke *et al*.[194] observed *in situ* GB sliding and grain rotation near the tips of opening cracks in nc-Au films. Shan *et al*.[196–198] and Wang *et al*.[203] reported on evident grain rotation in nc-Ni films deformed by *in situ* TEM tensile straining. Similar observations were made by Sergeeva *et al*.[199–201] in nc-Ni_3Al. The authors also noted that the mechanism of cooperative grain boundary sliding, which dominates in superplastic deformation of NCMs, is associated with sliding and rotation of entire grain groups. Yagi *et al*.[202] studied the surface morphology and the crystallographic texture of nc-Au and nc-Cu after creep deformation and concluded that grain rotation takes place along the localized grain boundary sliding during creep deformation. Wang *et al*.[203] observed that rotation of an individual grain is accompanied by rotation and further coalescence of neighbouring grains, which resulted in grain growth. Zizak *et al*.[204,205] irradiated nc-Ti layers at room temperature with Au ions and studied the bombardment-induced texture changes. They registered that 'during off-normal irradiation, the nanocrystals undergo grain alignment and rotation up to ~90° at the highest ion fluence'.[204]

Recent computer simulations have also manifested the rotational plastic deformation in NCMs with finest grains (average grain size from 5 to 7 nm).[157,206–210] Both the molecular dynamics[206] and quasicontinuum (molecular statics)[207–209] methods were used to simulate the evolution of atomic structure of NCMs in nc-Au[206] and nc-Al[207–209] under spherical nanoindenter. Among some other mechanisms of plasticity, the authors have observed the GB sliding accompanied by grain rotation and coalescence. Shimokawa *et al*.[157] evaluated the molecular dynamics simulation of nc-Al under tensile loading and also the fixed relative rotation of some neighbouring grains. Monk and Farkas[210] used the same method for studying the deformation behavior of nc-Ni nanowires under tension. They observed grain growth accompanied by grain rotation and measured the rotation angle of a sample grain in the center of the nanowire as a function of time for different strain rates. Their 'data show that the grain rotation speed varies

significantly with strain rate, indicating again that it is not a time controlled thermal process and is mostly driven by the strain itself'.[210]

Summarizing the results of experiments and computer simulations, one can conclude that stress- and strain-driven grain rotation is a typical mechanism of plastic deformation in NCMs with finest grains, which is accompanied by GB sliding and can lead to grain coalescence. To date there are a number of theoretical models which describe the gradual change in GB misorientation angles in the course of grain rotation. The earlier models[211–213] were aimed at the analyses of energetics of splitting of GB disclinations into smaller-strength GB disclinations. It was shown that the split arrangements are always more energetically preferable than the initial disclinations. However these models did not include any mechanism of disclination motion along GBs. Later it was suggested that motion of GB disclinations could be realized through emission of lattice perfect (Fig. 12.16) and partial (Fig. 12.10 (b)) dislocations into adjacent grains.[149,150,166,214,215] This

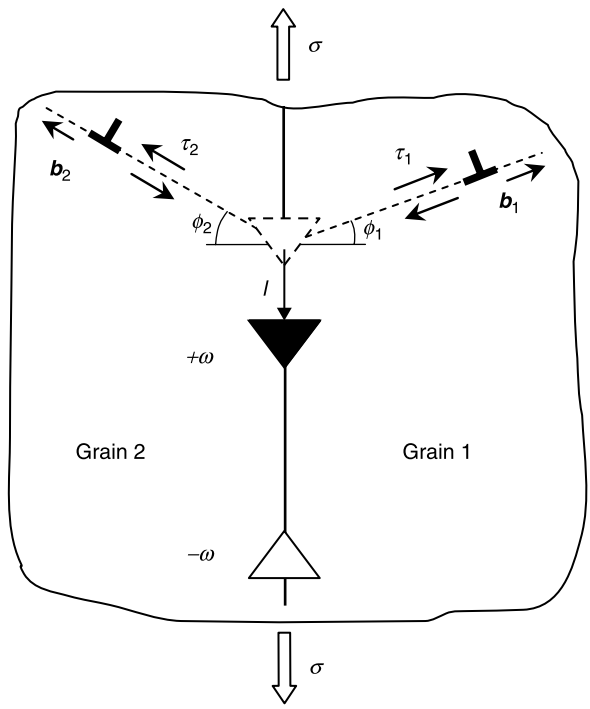

12.16 Stress-driven displacement of the wedge disclination (black triangle) with the strength $+\omega$ from its initial position (dashed triangle) by the distance l is accompanied by the emission of two lattice dislocations with Burgers vectors $\boldsymbol{b}_1$ and $\boldsymbol{b}_2$. The $+\omega$-disclination moves along the grain boundary plane towards another disclination (white triangle) with the strength $-\omega$. See Gutkin *et al.*[150] for details.

mechanism seems to be more appropriate for NCMs, which may contain only few lattice dislocations inside the grains, than the earlier proposed mechanism[66,216] of GB disclination motion through absorption of lattice dislocations from adjacent grains, which is appropriate for microcrystalline metals[216,217] containing a high density of lattice dislocations. The scheme that illustrated the contribution of grain rotation, which is realized through motion of GB disclination dipoles, to plastic deformation of a NCM, was presented by Ovid'ko.[218]

The above-mentioned theoretical models manifest interplay between the translational (glide of lattice dislocations) and rotational (motion of GB disclinations) modes of plastic deformation in NCMs. For the case where the translational mode is mainly represented by GB sliding (smallest nanograins and/or superplastic deformation), another model (Fig. 12.17) was suggested.[219] Its main idea is as follows. GB sliding occurs via the glide of GB dislocations with Burgers vectors, which are parallel to the GB planes along which these dislocations glide (Fig. 12.17 (b)). Triple junctions of GBs serve as obstacles for the GB dislocation motion. GB dislocations stopped at a triple junction are capable of being split into climbing GB dislocations (Fig. 12.17 (c)). When this process repeatedly occurs at a triple junction, it results in the formation of two walls of GB dislocations climbing along the GBs adjacent to the triple junction. The climbing GB dislocation walls cause the rotational deformation, in which case the repeatedly occurring splitting of gliding GB dislocations at the triple junction provides the crossover from the GB sliding to the rotational deformation mode (Fig. 12.17 (c), (d)). This process can be spread over the grain, which has to rotate on an angle as a whole (Fig. 12.17 (e)). Thus, the stopped GB sliding can stimulate plastic rotation of the neighbouring grain. Obviously this mechanism may only be effective under the condition of intensive GB diffusion of vacancies, which must be capable of providing the necessary velocity of GB dislocation climb. Analysing this model from a thermodynamic point of view, the authors[219] concluded that the transition from GB sliding to rotational deformation becomes energetically favourable when the external shear stress achieves its critical value, and this depends on the elastic properties of the NCM, the structure of its GBs, its grain size and its shape. Smaller grains require smaller critical stress to rotate.

Recent progress in theoretical modeling of rotational deformation in NCMs is mainly related with elaboration of dislocation–disclination models of grain refinement of polycrystalline metals under severe plastic deformation,[220–222] interplay between GB sliding and grain rotation[223–225] leading to the inverse Hall–Petch relationship in the range of smallest grain sizes,[223,224] and GB migration[95,96,226–230] and the formation of immobile disclinations whose strengths gradually increase during deformation as a result of grain boundary sliding and diffusion,[231] as special mechanisms of rotational plasticity. Some of these models[220–224] have been reviewed extensively by Romanov and Kolesnikova.[29] The models[226–230] are considered in more detail in Section 12.3.5.

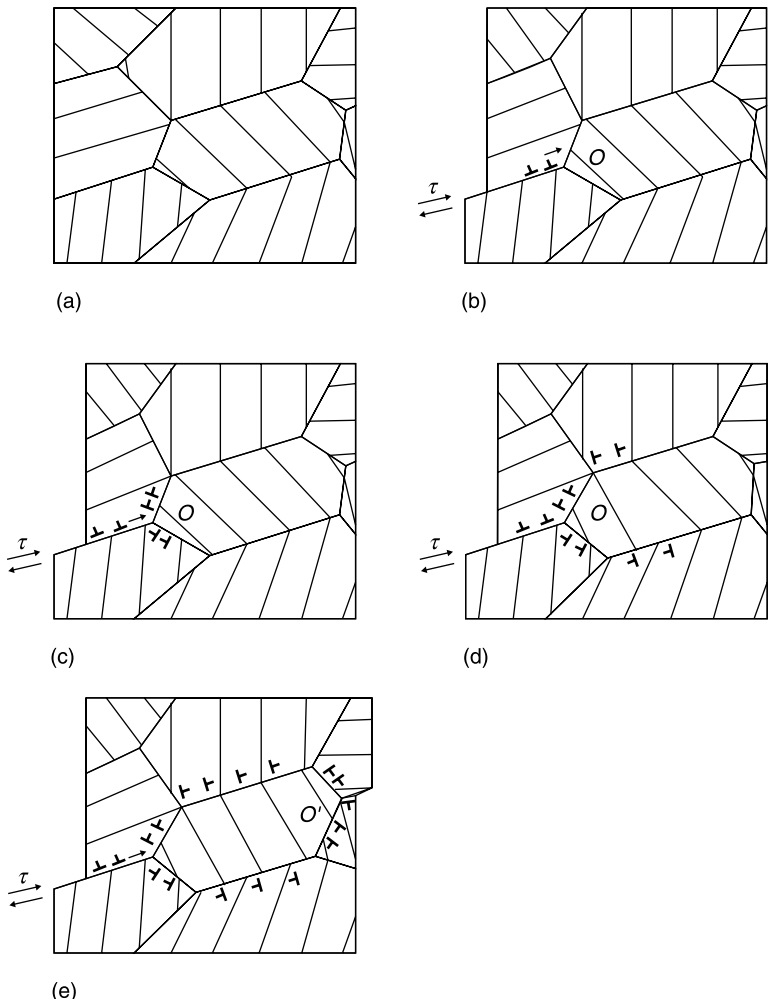

12.17 Combined action of grain boundary sliding and rotational deformation mode. (a) Nanocrystalline specimen in a non-deformed state. (b) Grain boundary sliding occurs via motion of gliding grain boundary dislocations under shear stress action. (c) Gliding dislocations split at triple junction O of grain boundaries into climbing dislocations. (d) The splitting of gliding grain boundary dislocations repeatedly occurs causing the formation of walls of grain boundary dislocations whose climb is accompanied by crystal lattice rotation in a grain. (e) Climbing dislocations reach triple junction *O′* where they converge into gliding dislocations causing further grain boundary sliding.

Alternative approaches to theoretical modeling of grain rotation in NCMs have been represented by Kim *et al*.[232] and Yang and Yang.[233] These authors consider the kinetics and size effects of GB sliding and grain rotation driven by both GB energy and external stress. Ignoring the underlying structural mechanisms of GB

sliding and grain rotation, they operate with continuum mechanics in terms of viscous GB gliding and GB diffusion as accommodation mechanisms. Due to its relative simplicity and high effectiveness, this approach looks rather attractive and fruitful although it does not allow one to visualize the structural mechanisms of grain rotation.

12.3.4 Mechanisms of strengthening and softening under superplasticity

The superplasticity of NCMs has attracted much attention in the past decade (see original papers[234–241] and reviews[99,101,108,118,121,122,242]). It has been found that the superplasticity in these materials is reached at lower temperatures and higher strain rates, offering strong possibilities for industrial application of this effect. Moreover, it has been discovered that the strength of a material increases significantly in the course of superplastic deformation. The yield stress and the hardening effect become especially great during deformation of NCMs, with an average grain size of about 50 nm. In this case, the stress–strain curves are bell-shaped, and demonstrate the presence of well-defined long hardening and softening stages.

Among the main mechanisms of plasticity operating in NCMs (see Fig. 12.3), the GB sliding (in combination with accommodation mechanisms, such as GB migration and lattice sliding near GBs) is believed to be the dominant mechanism of superplastic deformation in NCMs.[101,241] Therefore, the unusual effects of NCM hardening in the initial stage of superplastic deformation and subsequent softening, as well as very high values of the yield stress, can be due to the specific features of GB sliding. These features were described in theoretical models.[243–245] First, we considered a situation near an isolated triple junction of GBs along which GB dislocations glide under an external shear stress τ (Fig. 12.18). Following the models,[243,244] numerous acts of transfer of GB dislocations across the triple junction results in an increase in the Burgers vector of the difference sessile dislocation in the triple junction, which increases the critical stress τ_c necessary for dislocation transfer across the triple junction and hence leads to local strengthening. At the same time, the accompanying local migration of GBs leads to an increase in the angle a between the GB planes (adjacent to the triple junction), which decreases τ_c and hence leads to local softening.

The competition between the strengthening and the softening effects is capable of crucially influencing the deformation behavior of NCMs exhibiting high strain-rate superplasticity. In particular, superplastic deformation regime is realized if the strengthening dominates over the softening during the first extensive stage of deformation (characterized by a plastic strain of hundreds of percent). This strengthening prevents the necking and is responsible for an increase of the flow stress that drives the movement of GB dislocations. With rising plastic strain, local GB migration arranges GB planes to be tentatively parallel to each other in some local regions of a loaded sample. As a result, local softening becomes

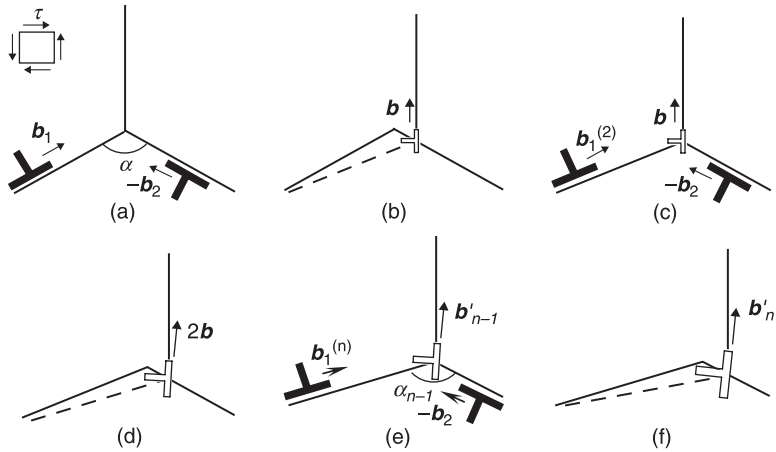

12.18 Numerous acts of transfer of GB dislocations across a triple junction and accompanying local migration of GBs leads to an increase in the angle α. (a) Initial (0th) state of defect configuration; two gliding GB dislocations move towards the triple junction. (b) Sessile dislocation with the Burgers vector $\boldsymbol{b}$ is formed; triple junction is displaced by the vector $\boldsymbol{b}_2$ from its initial position. (c) Generation of two new gliding GB dislocations that move towards the triple junction. (d) New sessile dislocation is formed; the triple junction is transferred by the vector $2\boldsymbol{b}_2$ from its initial position. (e) The nth generation of two new gliding GB dislocations that move towards the triple junction. (f) The nth sessile dislocation is formed; the triple junction is transferred by the vector $n\boldsymbol{b}_2$ from its initial position.

substantial, which causes gradual macroscopic softening inherent in the second stage of superplastic deformation of NCMs.

Secondly, we expanded these models by taking into account the effect of neighbouring triple junctions and the possible accommodation of the GB defect structure via emission of lattice dislocations (Fig. 12.19).[245] In the model used, perfect lattice dislocations are emitted from triple junctions when Burgers vectors of sessile triple-junction dislocations reach critical values. After the first emission of a perfect lattice dislocation, the strength of the sessile dislocation again increases gradually. When its Burgers vector reaches a new critical value, a lattice dislocation is emitted again. A detailed examination of these processes allowed us to numerically calculate the strain–stress dependence shown by the solid curve in Fig. 12.20,[245] for Al with the grain size of 100 nm. The dashed line represents experimental data.[239] It can be seen that the theoretical and experimental values are close to each other. The theoretical curve is serrated due to the contribution from lattice sliding to the superplastic strain. Each elementary event of lattice sliding causes a drop in the critical stress, thereby leading to local softening.

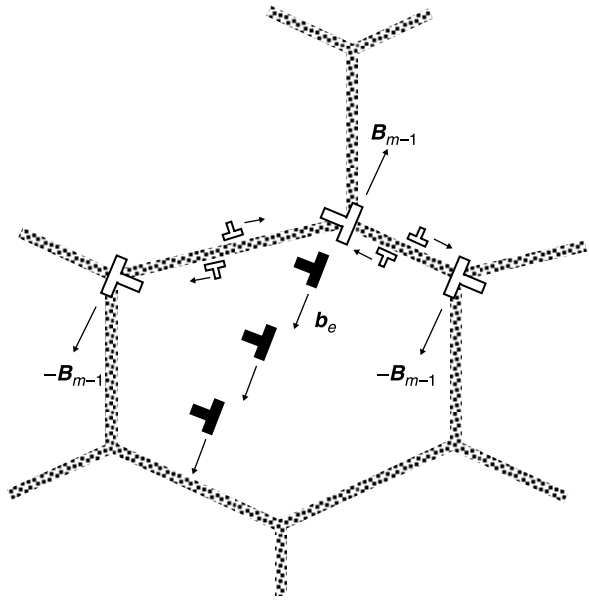

12.19 Emission of lattice dislocations with the Burgers vector $\boldsymbol{b}_e$ from a sessile dislocation with the Burgers vector $\boldsymbol{B}_{m-1}$ in a triple junction on the *m*th transfer of GB dislocations across the triple junction.

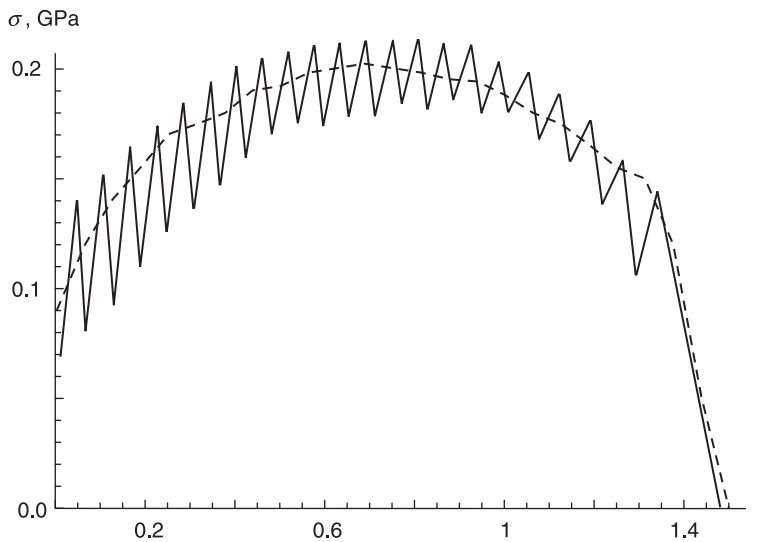

12.20 External stress σ as a function of the total plastic strain ε.

Further theoretical investigation of defect structure evolution near triple junctions of GBs during GB sliding has been evaluated recently by Ovid'ko and Sheinerman.[246] The authors have taken into account the formation of disclination dipoles near triple junctions and the partial relief of disclination stresses due to GB diffusion. As the first process increases the strain hardening, while the second one decreases it, these factors could also be used in further theoretical models of superplasticity.

12.3.5 Athermal stress-induced grain growth

In recent years, particular attention has been focused on the grain growth during plastic deformation of ultrafine-grained[247–253] and nanocrystalline[72,203,249–269] metals and alloys at room[72,203,249–269] and cryogenic[253–255] temperatures. Experimental studies on ultrafine-grained pure Al[247,249–252] and Cu[248,253] and Al-Mg alloys[250,251] and on nanocrystalline pure Al,[249–252,259–261,269] Cu,[253–255,267] Ni,[203,256–258,267,268] Pd[72] and Co-P[263,264] and Ni-Fe[264–266] alloys have shown that the grain growth is possible during nano-[249–252,257] and micro-indentation[253–255] of thin films and torsion of them under high pressure,[72,256] during compression of powder,[247] micropillars[258] and macroscopic samples,[248,265] during cold-rolling,[268] and, finally, during uniaxial tension of thin films[203,259–262,269] and bulk planar samples.[263,264,266] For an understanding of the physical nature of this phenomenon, the following experimental facts are of importance:

(i) At cryogenic temperatures, grains grow more rapidly than at room temperature.[254]

(ii) The grain growth is the most intensive in the regions of a sample where the elastic stress and its gradient are the largest (e.g. under a nanoindenter[249–252,257] or in the immediate vicinity of a microindenter,[253–255] near the tip of a slowly developing crack,[259,262] in the surface layer of a sample in the vicinity of a neck forming under tension,[266] or near specially prepared holes under tension[269]).

(iii) The grain growth is completely suppressed[250] or reduced[261,263–266] in the presence of impurities.

(iv) During grain growth, not only the grain size but also the character of the grain size distribution are changed; the distribution is broadened and sometimes becomes bimodal,[254,259,264] with larger submicron grains occupying up to 15% of the volume[254] and fine nanograins surrounding them.

(v) The grain growth occurs at relatively low nanoindentation rates[257] and during microindentation in the creep mode,[253–255] at relatively high compression rates (~10^{-3}–10^{-1} s^{-1} [258] and 10^{-3} s^{-1} [265]), and at widely ranged tension rates (~10^{-5} s^{-1},[259–261] 10^{-3} s^{-1},[260,263] 10^{-5}–10^{-2} s^{-1},[264] 10^{-2} s^{-1} [266]).

(vi) The grain growth somewhat decreases the ultimate strength, but it significantly increases the ultimate tensile strain (up to 25% in pure nc-Al[259] and up to 7.2% in the nc-Ni-Fe alloy[266]), which is accompanied by noticeable hardening and the formation of dislocation structures in coarse grains. In micropillars of pure nc-Ni under uniaxial compression, ultrahigh plasticity

(up to 200% of the true strain) was observed at a flow stress of 2.0–2.4 GPa, which was accompanied by softening (due to equiaxial grain growth) followed by hardening caused by the elongation of grown grains and the accumulation of dislocations and twins in them.[258]

(vii) With increasing duration of holding of a sample under indenter, the low-angle GBs were observed to increase in number, especially at cryogenic temperatures.[255] In submicron-sized grains grown during severe plastic deformation, subgrains were observed, which, in turn, were filled with dislocation cells.[256]

The authors[72,203,249–269] believe that the above results unambiguously indicate the athermic character of grain growth, which occurs under elastic stresses forming at earlier stages of plastic flow. The process of grain growth is inhomogeneous over a cross-section of the sample; indeed, the grains that are located in places of concentrated stresses and, in addition, have a favourable orientation, increase in size. When the growing grains become a few hundred nanometers in size, the plasticity mechanisms typical of low-temperature deformation of coarse-grained metals begin to operate in them. For example, in copper, dislocation glide and the formation of dislocation pile-ups were observed at room temperature, and deformation twinning at a cryogenic temperature (77 K).[255] Thus, the grain growth during plastic deformation increases the plasticity of NCMs, while the flow stress remains high at low temperatures and relatively high loading rates, which is very important for practical applications.[252]

Recent computer simulations[157,207,208,210,270–274] have shown that low-temperature stress-induced grain growth in NCMs is athermal. Its basic mechanisms are found to be stress-induced migration of GBs and their triple junctions, GB sliding, grain rotation and coalescence (see also Section 12.3.3). In particular, all of these mechanisms were observed to operate simultaneously in model samples of nc-Al[208] and Ni[210] with a mean grain size of 7 and 5 nm, respectively, when nanograins rotated through GB sliding under nanoindentation[208] or uniaxial tension.[210] The atomic mechanisms of motion of high-angle GBs have been considered in a number of recent works.[275–281]

Also, stress-induced GB migration and athermal grain growth have been described theoretically with the aid of dislocation-disclination models.[95,96,152–154,226–230,282] For example, Bobylev *et al.*[152–154] have studied the dynamics and decay of a low-angle tilt boundary under an applied shear stress τ (see Section 12.3.1). It was shown that, as the stress τ increases, the tilt boundary is first bent and then shifts to a new position corresponding to the applied stress. At a certain critical stress proportional to the misorientation angle θ of the boundary, it becomes unstable and glides irreversibly. The decay of one such boundary significantly decreases the critical stress for decay of neighbouring low-angle boundaries. As a result, the chain decay of the neighbouring boundaries occurs and the grains separated by them coalesce. The static model of the escape of dislocations from an infinite straight dislocation wall developed by Li[282] also

permits one to estimate the critical stress for boundary decay, which is proportional to θ. The stress at which an intrinsic dislocation of a low-angle boundary (with $\theta = 0.1$ ($\approx 5.7°$)) breaks away from it (estimated from this model to be about 2 GPa for Fe)[282] is not far greater than that obtained from dynamic calculations (1.53 GPa).[152–154] The model of Li[282] also gives lower values of the critical stress for the decay of a boundary in the case where a few intrinsic or extrinsic dislocations break away simultaneously from it. However, the description of the boundary decay assuming that only single dislocations move while the positions of the other dislocations remain unchanged seems incorrect.

Gutkin and Ovid'ko[226] proposed a continuum disclination model for describing the migration of an arbitrary tilt GB. A migrating GB was approximated by a biaxial dipole of partial wedge disclinations capable of moving under an applied shear stress τ in the elastic field of a similar disclination dipole of opposite sign that forms when the GB breaks away from the neighbouring GBs (i.e. at the moment when triple GB junctions transform into double junctions) (Fig. 12.21).

It was shown that there are two modes of GB migration. When the applied stress reaches the first critical value:

$$\tau_{c1} \approx \frac{D\omega b}{2a} \ln\frac{2a}{b}, \qquad [12.7]$$

where $D = G/[2\pi(1-\nu)]$, G is the shear modulus, ν is the Poisson ratio, ω is the disclination strength equal to the misorientation angle of the migrating GB, $2a$ is the length of the GB and b is the interatomic distance, the GB begins to migrate in the stable mode in which its equilibrium position is determined by a stress level $\tau \geq \tau_{c1}$. When the stress τ reaches the second critical value:

$$\tau_{c2} \approx 0.8D\omega, \qquad [12.8]$$

the GB migration becomes unstable; the equilibrium position of the GB disappears, and the GB migration no longer depends on τ. For pure nc-Al with grain size d ranging from 30 to 100 nm, the stress τ_{c1} ranges from 7.6 to 23.5 MPa for $\omega = 5°$ and from 46.5 to 144 MPa for $\omega = 30°$. The stress τ_{c2} proves to be far greater, namely, 0.4 GPa for $\omega = 5°$ and 2.5 GPa for $\omega = 30°$, irrespective of the grain size. We note that, in thin nc-Al films under tension, grains begin to grow intensively over the range of true tensile stresses from 130 MPa for $d \approx 90$ nm to 190 MPa for $d \approx 40$ nm,[259,260] which correspond to the maximum values of τ from 65 to 95 MPa lying in the range $\tau_{1c} < \tau < \tau_{c2}$ for GBs with a misorientation angle $\omega = 5°$ and in a part of this range for GBs with $\omega = 30°$. Computer simulations of nanoindentation of nc-Al films with a mean grain size of 7 nm showed[208] that the migration of a low-angle tilt boundary with a misorientation angle of 13.5° becomes unstable under local shear stresses exceeding the estimated value 0.7 GPa obtained from equation [12.8].

Recently the model[226] has been extended to the case of collective migration of the two opposite boundaries of a grain.[227,228] We have considered the stress-induced

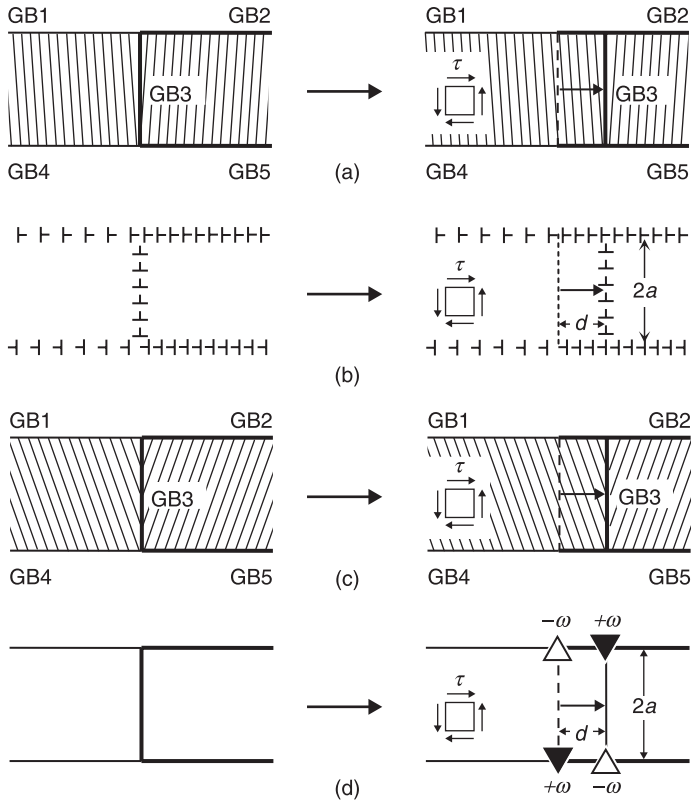

12.21 Stress-induced migration of a low-angle (a,b) or high-angle (c,d) grain boundary (GB3) as a mechanism of rotational deformation realized through the glide of a wall of lattice dislocations (b) or motion of a dipole of wedge disclinations (d), respectively.

grain growth in a model nc-sample under a tensile stress σ (Fig. 12.22) and analysed in detail the situation with one pair of interacting GBs (Fig. 12.23). We have shown that two critical stresses, τ_c and τ_m, control the behavior of migrating GBs. When the external shear stress τ reaches τ_c, opposite GBs start to migrate to each other, their migration is stable, and their equilibrium positions are determined by $\tau \geq \tau_c$. When $\tau \geq \tau_m >> \tau_c$, the GBs meet. Then the following regimes of cooperative migration are possible at $\tau > \tau_m$, depending on τ level and GB characteristics: 1) GBs annihilate in the very partial case where their misorientations are equal by magnitude and opposite in sign, 2) one GB captures another GB and makes it migrate together in one direction under a moderate τ, 3) GBs coalesce and stand at a local equilibrium position, 4) GBs can overcome their mutual attraction and migrate in opposite directions under a very high τ. In all cases, GB migration leads to unstable growth of a grain by annexing parts of its neighbours.

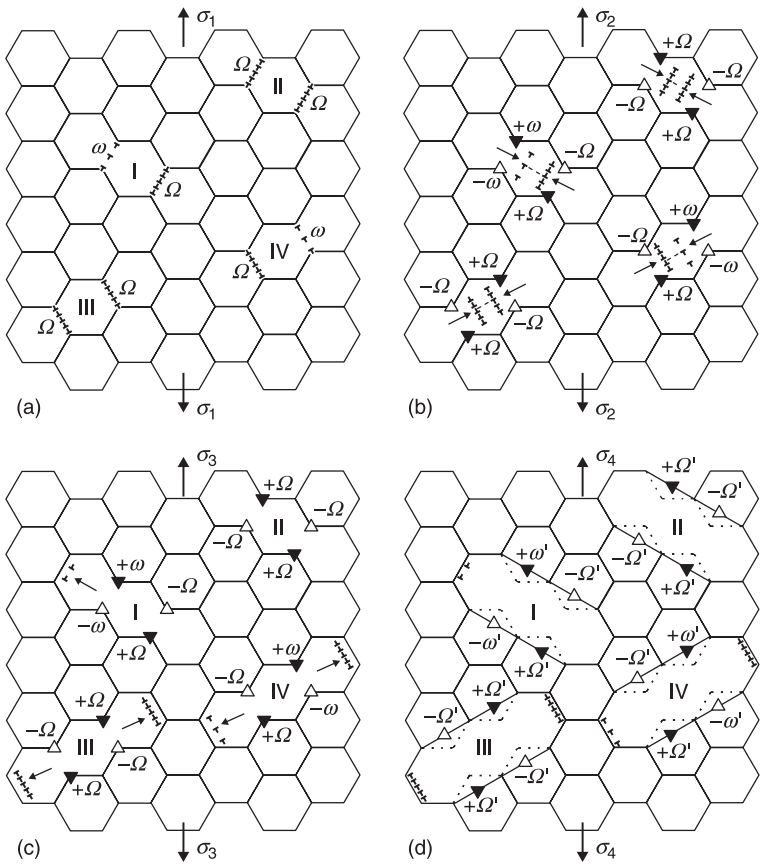

12.22 Grain growth through collective GB migration in a model NCM under uniaxial tension: (a) the initial state of tilt boundaries with misorientation angles ω and Ω at a low tensile stress σ_1; (b) at a stress $\sigma_2 > \sigma_1$, the boundaries begin to migrate into grains I–IV and partial wedge disclinations with strengths $\pm\omega$ and $\pm\Omega$ appear in the remaining double junctions and form dipole and quadrupole structures; (c) at a higher stress $\sigma_3 > \sigma_2$, some boundaries annihilate partially (grain I) or completely (grain II), while others pass through each other and stop only near the next boundaries (grains III, IV); (d) smoothing of the boundaries of the enlarged grains I–IV at a stress $\sigma_4 \geq \sigma_3$.

The model[226] has also been extended to the cases of GB migration and grain nucleation near cracks.[95,96,229] It was shown that these processes result in moderate enhancement of fracture toughness[96] and in an increase in the equilibrium lengths of the cracks, thus diminishing the probability of their development.[229] On the other hand, the stress concentration provided by cracks leads to a decrease in the critical stresses τ_{c1} and τ_{c2}.[95]

Bobylev and Ovid'ko[230] have considered GB migration in hexagonal grains and found that, depending on the angle between the mobile and immobile GBs,

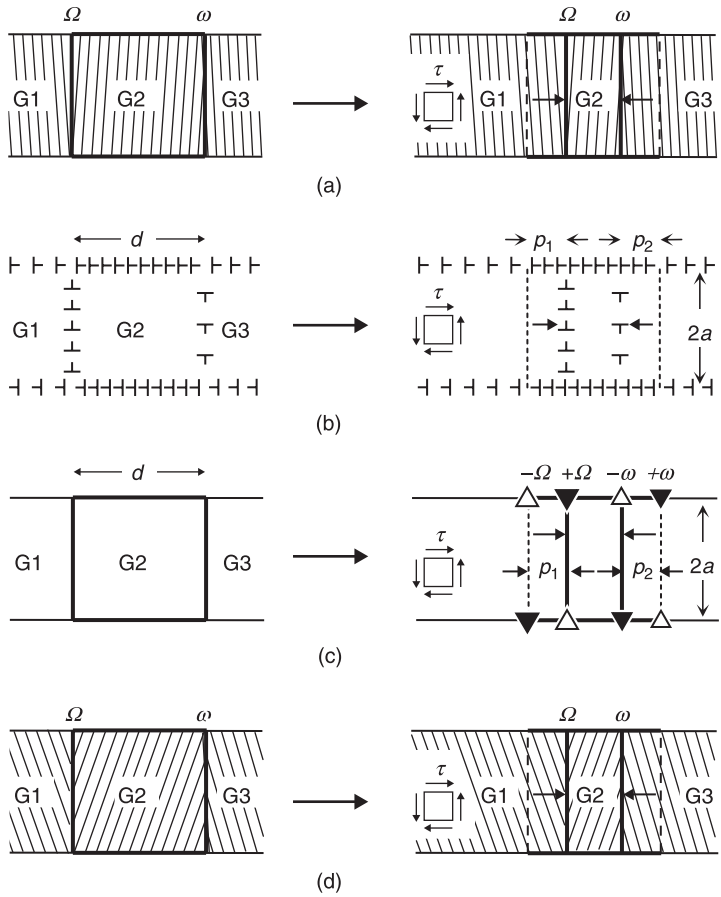

12.23 Collective migration of (a, b) low-angle and (c, d) high-angle tilt boundaries separating grains *G*1–*G3* under applied shear stress τ: (a, d) geometrical models and (b, c) dislocation and disclination models, respectively.

GBs migrate more easily (at a lower stress level) compared to the previously examined situation[226] with rectangular grains. The difference in the stress may reach a value of ~20 to 30%. The authors[230] have concluded that 'geometry of triple junctions crucially influences their mobility and thereby controls the stress level needed to drive migration of GBs and their triple junctions in deformed nanocrystalline materials'.

12.4 Conclusions and future trends

We have considered some analytical theoretical models that describe elastic strains and plastic deformation phenomena in NCMs. Most of these models are

based on the theory of defects, a unified concept that allows one to describe the structure, the elastic fields and the mechanisms of plastic deformation from a unique physical viewpoint. Based on the results of such theoretical modeling, one can formulate the following general conclusions:

(i) Due to their structural and scale features, NCMs always contain many elastic-strain sources and stress concentrators that are capable of initiating various mechanisms of plastic deformation under external loading. Most of the stress sources and concentrators are defects localized at/near GBs. At the same time, most of these defects can act as carriers of plastic deformation. As a result, GB-mediated mechanisms of plasticity dominate over other possible mechanisms in fine-grained NCMs.

(ii) The GB mediated mechanisms of plasticity are emissions of partial and perfect lattice dislocations and twins from GBs; mass transfer along GBs and their triple junctions; GB sliding, decay and migration; grain rotation, growth and refinement. The present review demonstrates that most of these deformation mechanisms can be analysed theoretically within a unified energy approach. In doing so, one can calculate and analyse some critical values of the applied stress, which control the barrier-less activation of the deformation mechanisms and their transition from the stable regime of development to its unstable regime. Using these results, one can sometimes conclude which deformation mode is preferable in given conditions. When possible, the comparison of theoretical estimates with available experimental data and results of computer simulations shows rather good accordance.

(iii) Due to the distribution in grain size, different mechanisms of plastic deformation can dominate in different grains; these mechanisms can also compete within the same grains. Interplay between different mechanisms of plasticity commonly occurs in NCMs. Theoretical modeling of this interplay seems to be a good and important challenge at present.

This chapter has concentrated mainly on quasistatic theoretical models. Meanwhile, there are a number of models developed for ultrafine-grained and nanocrystalline materials within the evolutional dislocation kinetics[78,120,283,284] and discrete dislocation dynamics.[285,286] It seems that incorporating GB dislocation and disclination terms to these models may be a future trend in this field. One more future trend is the wider use of elastic fields of defects calculated in the framework of the strain-gradient elasticity,[30,31,84] which allows one to avoid the classical singularities in elastic fields of defects and their interactions. Some examples of applying this theory to dislocation behavior in freestanding[287] and in/near embedded nanowires[288,289] have recently been demonstrated. Future theoretical models are also expected to describe in more details the interplay between dislocation–disclination and GB diffusion modes of plastic deformation, and between the mechanisms of plasticity and fracture as well.

12.5 Sources of further information and advice

Further information on the topics under discussion in this chapter can be taken from monographs,[78,131–133] reviews[1,2,10,17–22,29,59,97–130] and other references listed in Section 12.7. The most useful sources of current information are such materials science and physical journals as *Acta Materialia*, *Applied Physics Letters*, *Journal of Materials Research*, *Journal of Materials Science*, *Materials Science and Engineering A*, *Nature Materials*, *Philosophical Magazine*, *Philosophical Magazine Letters*, *Physical Review B*, *Physical Review Letters*, *Physics of Solid State*, *Progress in Materials Science*, *Reviews on Advanced Materials Science*, *Science*, *Scripta Materialia*, etc.

12.6 Acknowledgements

The work was supported by the Russian Foundation of Basic Research (Grant No. 08–02–00304-a). I am deeply thankful to my friends and colleagues E.C. Aifantis, S.V. Bobylev, A.A. Fedorov, A.L. Kolesnikova, K.N. Mikaelyan, N.F. Morozov, I.A. Ovid'ko, C.S. Pande, A.E. Romanov, A.G. Sheinerman and N.V. Skiba for helpful discussions and collaboration.

12.7 References

1 Gleiter H. Prog Mater Sci 1989;33: 223.
2 Gryaznov V.G., Trusov L.I. Prog Mater Sci 1993;37: 289.
3 Wunderlich W., Ishida Y., Maurer R. Scr Metall Mater 1990;24: 403.
4 Herr U., Jing J., Birringer R., Conser U., Gleiter H. Appl Phys Lett 1987;50: 472.
5 Schaefer H-E., Wurshum R. Phys Lett A 1987;119: 370.
6 Wurshum R., Scheytt M., Schaefer H-E. Phys Stat Sol A 1987;102: 119.
7 Zhu X., Birringer R., Herr U., Gleiter H. Phys Rev B 1987;35: 9085.
8 Haubold T., Birringer R., Lengeler B., Gleiter H. Phys Lett A 1989;135: 461.
9 Jorra E., Franz H., Peisl J., Wallner G., Petry W., Haubold T., Birringer R., Gleiter H. Phil Mag B 1989;60: 159.
10 Valiev R.Z., Islamgaliev R.K., Alexandrov I.V. Prog Mater Sci 2000;45: 103.
11 Cammarata R.C. Prog Surf Sci 1994;46: 1.
12 Nicholson M.M. Proc Roy Phys Soc Lond A 1955;228: 490.
13 Ono S., Kondo S. Molecular theory of surface tension in liquids. Berlin: Springer; 1960.
14 Jia M., Lai Y., Tian Z., Liu Y. Modelling Simul Mater Sci Eng 2009;17: 015006.
15 Marks L.D. Rep Prog Phys 1994;57: 603.
16 Gillet M. Surf Sci 1977;67: 139.
17 Martin T.P. Phys Rep 1996;273: 199.
18 Hofmeister H. Cryst Res Technol 1998;33: 3.
19 Gryaznov V.G., Heydenreich J., Kaprelov A.M., Nepijko S.A., Romanov A.E., Urban J. Cryst Res Technol 1999;34: 1091.
20 Yacamán M.J., Ascencio J.A., Liu H.B., Gardea-Torresdey J. J Vac Sci Technol B 2001;19: 1091.
21 Hofmeister H. In: Nalwa H.S., editor. Encyclopedia of nanoscience and nanotechnology, vol. 3. Stevenson Ranch: American Scientific Publishers; 2004; p.431.

22 Elechiguerra J.L., Reyes-Gasga J., Yacaman M.J. J Mater Chem 2006;16: 3906.
23 Vikarchuk A.A., Volenko A.P. Phys Solid State 2005;47: 352.
24 Yasnikov I.S., Vikarchuk A.A. Phys Solid State 2006;48: 1433.
25 Yasnikov I.S. Phys Solid State 2007;49: 1224.
26 Yasnikov I.S., Vikarchuk A.A., Denisova D.A., Gryzunova N.N., Tsybuskina I.I. Tech Phys 2007;52: 1328.
27 de Wit R. J Phys C: Sol State Phys 1972;5: 529.
28 Galligan J.M. Scr Metall 1972;6: 161.
29 Romanov A.E., Kolesnikova A.L. Prog Mater Sci 2009;54: 740.
30 Gutkin M.Yu., Aifantis E.C. Phys Solid State 1999;41: 1980.
31 Gutkin M.Yu. Rev Adv Mater Sci 2000;1: 27.
32 Povstenko Yu.Z. Int J Engng Sci 1995;33: 575.
33 Zubov L.M. Nonlinear theory of dislocations and disclinations in elastic bodies. Berlin: Springer; 1997.
34 Lazar M. Phys Lett A 2003;311: 416.
35 Howie A., Marks L.D. Phil Mag A 1984;49: 95.
36 Dorogin L.M., Kolesnikova A.L., Romanov A.E. Tech Phys Lett 2008;34: 779.
37 Marks L.D. Phil Mag A 1984;49: 81.
38 Rodríguez-López J.L., Montejano-Carrizales J.M., Pal U., Sánchez-Ramírez J.F., Troiani H.E., García D., Miki-Yoshida M., José-Yacamán M. Phys Rev Lett 2004;92: 196102.
39 Gryaznov V.G., Kaprelov A.M., Romanov A.E., Polonskii I.A. Phys Stat Sol B 1991;167: 441.
40 Kolesnikova A.L., Romanov A.E. Tech Phys Lett 2007;33: 886.
41 Kolesnikova A.L., Romanov A.E. Phys Stat Sol RRL 2007;1: 271.
42 Panpurin S.N., Gutkin M.Yu. In: Proceedings of All-Russian Inter-University Scientific-Technical Conference of Students and PhD Students, 30 Nov–4 Dec 2009, St. Petersburg: Izdatel'stvo Politekhnicheskogo Universiteta, 2009; p.142, in Russian.
43 Li D.X., Ping D.H., Ye H.Q., Qin X.Y., Wu X.J. Mater Lett 1993;18: 29.
44 Huang J.Y., Wu Y.K., Ye H.Q. Acta Mater 1996:44: 1211.
45 Huang J.Y., Yu Y.D., Wu Y.K., Li D.X., Ye H.Q. J Mater Res 1997;12: 936.
46 Liao X.Z., Huang J.Y., Zhu Y.T., Zhou F., Lavernia E.J. Phil Mag 2003;83: 3065.
47 Liao X.Z., Zhao Y.H., Srinivasan S.G., Zhu Y.T., Valiev R.Z., Gunderov D.V. Appl Phys Lett 2004;84: 592.
48 Zhu Y.T., Liao X.Z., Valiev R.Z. Appl Phys Lett 2005;86:103112.
49 Cao A.J., Wei Y.G. Appl Phys Lett 2006;89: 041919.
50 Bringa E.M., Farkas D., Caro A., Wang Y.M., McNaney J., Smith R. Scr Mater 2008;59: 1267.
51 Shao Y.F., Wang S.Q. Scr Mater 2010;62: 419.
52 Saada G. Acta Metall 1979;27: 921.
53 Horita Z., Smith D.J., Furukawa M., Nemoto M., Valiev R.Z., Langdon T.G. J Mater Res 1996;11: 1880.
54 Horita Z., Smith D.J., Nemoto M., Valiev R.Z., Langdon T.G. J Mater Res 1998;13: 446.
55 Ranganathan S., Divakar R., Raghunathan V.S. Scr Mater 2001;44: 1169.
56 Huang J.Y., Zhu Y.T., Jiang H., Lowe T.C. Acta Mater 2001;49: 1497.
57 Huang J.Y., Liao X.Z., Zhu Y.T., Zhou F., Lavernia E.J. Phil Mag 2003;83: 1407.
58 Valiev R.Z., Sergueeva A.V., Mukherjee A.K. Scr Mater 2003;49: 669.
59 Koneva N.A. In: Altan B.S., editor. Severe plastic deformation: toward bulk production of nanostructured materials. New York: Nova Science Publishers; 2006; p.249.

60 Wu X.L., Zhu Y.T. Appl Phys Lett 2006;89: 031922.
61 Koneva N.A., Kozlov E.V., Popova N.A., Zhdanov A.N., Fedorischeva M.V. Mater Sci Forum 2008;584–586: 269.
62 Liu M.P., Roven H.J., Ungar T., Balogh L., Murashkin M., Valiev R.Z. Mater Sci Forum 2008;584–586: 528.
63 Sutton A.P., Balluffi R.W. Interfaces in crystalline materials. Oxford: Oxford Science Publications; 1996.
64 Likhachev V.A., Rybin V.V. Sov Phys – Solid State 1976;18:93.
65 Bollmann W. Phil Mag A 1984;49: 73.
66 Romanov A.E., Vladimirov V.I. In: Nabarro F.R.N., editor. Dislocations in solids, vol. 9. Amsterdam: North-Holland; 1992; p.191.
67 Rybin V.V., Zisman A.A., Zolotorevsky N.Yu. Acta Metall Mater 1993;41: 2211.
68 Languillaume J., Chmelik F., Kapelski G., Bordeaux F., Nazarov A.A., Canova G., Esling C., Valiev R.Z., Baudelet B. Acta Metall Mater 1993;41: 2953.
69 Valiev R.Z., Musalimov R.Sh. Phys Metals Metallogr 1994;78: 666.
70 Alexandrov I.V., Zhang K., Kilmametov A.R., Lu K., Valiev R.Z. Mater Sci Eng A 1997;234–236: 331.
71 Islamgaliev R.K., Chmelik F., Kuzel R. Mater Sci Eng A 1997;234–236: 335.
72 Ivanisenko Y., Kurmanaeva L., Weissmueller J., Yang K., Markmann J., Rösner H., Scherer T., Fecht H-J. Acta Mater 2009;57: 3391.
73 Godon A., Creus J., Cohendoz S., Conforto E., Feaugas X., Girault P., Savall C. Scr Mater 2010;62: 403.
74 Nazarov A.A., Romanov A.E., Valiev R.Z. Acta Metall Mater 1993;41: 1033.
75 Nazarov A.A., Romanov A.E., Valiev R.Z. Nanostruct Mater 1994;4: 93.
76 Nazarov A.A., Romanov A.E., Valiev R.Z. Nanostruct Mater 1995;6: 775.
77 Nazarov A.A., Romanov A.E., Valiev R.Z. Scr Mater 1996;34: 729.
78 Gutkin M.Yu., Ovid'ko I.A. Plastic deformation in nanocrystalline materials. Berlin: Springer; 2004.
79 Hahn H., Mondal P., Padmanabhan K.A. Nanostruct Mater 1997;9: 603.
80 Van Swygenhoven H., Spaczer M., Caro A. Acta Mater 1999;47: 3117.
81 Pozdnyakov V.A., Glezer A.M. Phys Solid State 2002;44: 732.
82 Markmann J., Bunzel P., Rösner H., Liu K.W., Padmanabhan K.A., Birringer R., Gleiter H., Weissmüller J. Scr Mater 2003;49: 637.
83 Hirth J.P., Lothe J. Theory of dislocations. New York: Wiley; 1982.
84 Kumar K.S., Suresh S., Chisholm M.F., Horton J.A., Wang P. Acta Mater 2003;51: 387.
85 Ovid'ko I.A., Sheinerman A.G. Acta Mater 2004;52: 1201.
86 Pozdnyakov V.A., Glezer A.M. Phys Solid State 2005;47: 817.
87 Kozlov E.V., Popova N.A., Ivanov Yu.F., Ignatenko L.N., Koneva N.A., Pekarskaya E.E. Ann Chim 1996;21: 427.
88 Ishida Y., Ichinose H., Kizuka T., Suenaga K. Nanostruct Mater 1995;6: 115.
89 Sanders P.G., Weertman J.R., Barker J.G. J Mater Res 1996;11: 3110.
90 Sanders P.G., Eastman J.A., Weertman J.R. Acta Metall 1998;46: 4195.
91 Agnew S.R., Elliott B.R., Youngdahl C.J., Hemker K.J., Weertman J.R. Mater Sci Eng A 2000;285: 391.
92 Ovid'ko I.A., Sheinerman A.G. Rev Adv Mater Sci 2006;11: 46.
93 Bobylev S.V., Morozov N.F., Ovid'ko I.A. Phys Solid State 2007;49: 1098.
94 Gutkin M.Yu., Ovid'ko I.A., Skiba N.V. Phil Mag 2008;88: 1137.
95 Morozov N.F., Ovid'ko I.A., Sheinerman A.G. Dokl Phys 2008;53: 144.

96 Ovid'ko I.A., Skiba N.V., Mukherjee A.K. Scr Mater 2010;62: 387.
97 Gleiter H. Acta Mater 2000;48: 1.
98 Gutkin M.Yu., Ovid'ko I.A., Pande C.S. Rev Adv Mater Sci 2001;2: 80.
99 Mohamed F.A., Li Y. Mater Sci Eng A 2001;298: 1.
100 Padmanabhan K.A. Mater Sci Eng A 2001;304–306: 200.
101 Mukherjee A.K. Mater Sci Eng A 2002;322: 1.
102 Gutkin M.Yu., Ovid'ko I.A. Rev Adv Mater Sci 2003;4: 79.
103 Kumar K.S., Van Swygenhoven H., Suresh S. Acta Mater 2003;51: 5743.
104 Tjong S.C., Chen H. Mater Sci Eng R 2004;45: 1.
105 Asaro R.J., Suresh S. Acta Mater 2005;53: 3369.
106 Han B.Q., Lavernia E.J., Mohamed F.A. Rev Adv Mater Sci 2005;9: 1.
107 Ovid'ko I.A. Int Mater Rev 2005;50: 65.
108 Ovid'ko I.A. Rev Adv Mater Sci 2005;10: 89.
109 Wolf D., Yamakov V., Phillpot S.R., Mukherjee A., Gleiter H. Acta Mater 2005;53: 1.
110 Kozlov E.V. In: Altan B.S., editor. Severe Plastic Deformation: Toward Bulk Production of Nanostructured Materials. New York: Nova Science Publishers; 2006; p.295.
111 Ma E. JOM 2006;58: 49.
112 Meyers M.A., Mishra A., Benson D.J. Prog Mater Sci 2006;51: 427.
113 Witkin D.B., Lavernia E.J. Prog Mater Sci 2006;51: 1.
114 Valiev R.Z., Langdon T.G. Prog Mater Sci 2006;51: 881.
115 Van Swygenhoven H., Weertman J.R. Mater Today 2006;9(5): 24.
116 Dalla Torre F.H., Gazder A.A., Pereloma E.V., Davies C.H.J. J Mater Sci 2007;42: 1622.
117 Dao M., Lu L., Asaro R.J., De Hosson J.T.M., Ma E. Acta Mater 2007;55: 4041.
118 Kawasaki M., Langdon T.G. J Mater Sci 2007;42: 1782.
119 Koch C.C. J Mater Sci 2007;42: 1403.
120 Malygin G.A. Phys Solid State 2007;49: 1013.
121 Sergeeva A.V., Mara N.A., Mukherjee A.K. Mater Sci Eng A 2007;463: 8.
122 Sergeeva A.V., Mara N.A., Mukherjee A.K. J Mater Sci 2007;42: 1433.
123 Valiev R.Z. J Mater Sci 2007;42: 1483.
124 Wei Q. J Mater Sci 2007;42: 1709.
125 Zhang H.W., Hansen N. J Mater Sci 2007;42: 1682.
126 Kozlov E.V., Zhdanov A.N., Koneva N.A. Phys Mesomech 2008;11: 42.
127 Van Swygenhoven H. Mater Sci Eng A 2008;483–484: 33.
128 Zhilyaev A.P., Langdon T.G. Prog Mater Sci 2008;53: 893.
129 Andrievski R.A., Glezer A.M. Physics – Uspekhi 2009;52: 315.
130 Pande C.S., Cooper K.P. Prog Mater Sci 2009;54: 689.
131 Gusev A.I., Rempel A.A. Nanocrystalline materials. Cambridge: Cambridge International Science Publishing; 2004.
132 Koch C.C., Ovid'ko I.A., Seal S., Veprek S. Structural nanocrystalline materials: fundamentals and applications. Cambridge: Cambridge University Press; 2007.
133 Cherkaoui M., Capolungo L. Atomistic and continuum modeling of nanocrystalline materials: deformation mechanisms and scale transition. Berlin: Springer; 2009.
134 Gutkin M.Yu., Ovid'ko I.A. Appl Phys Lett 2006;88: 211901.
135 Gutkin M.Yu., Ovid'ko I.A. Acta Mater 2008;56: 1642.
136 Xu G., Argon A.S. Phil Mag Lett 2000;80: 605.
137 Gutkin M.Yu., Ishizaki T., Kuramoto S., Ovid'ko I.A. Acta Mater 2006;54: 2489.

138 Cui J.P., Hao Y.L., Li S.J., Sui M.L., Li D.X., Yang R. Phys Rev Lett 2009;102: 045503.
139 Joós B., Ren Q., Duesbery M.S. Phys Rev B 1994;50: 5890.
140 Lu G., Kioussis N, Bulatov V.V., Kaxiras N. Phys Rev B 2000;62: 3099.
141 Bernstein N., Tadmor E.B. Phys Rev B 2004;69: 094116.
142 Van Swygenhoven H., Derlet P.M., Frøseth A.G. Nat Mater 2004;3: 399.
143 Lazar P., Podloucky D.C. Phys Rev B 2007;75: 024112.
144 Wang Y.M., Bringa E.M., McNaney J.M., Victoria M., Caro A., Hodge A.M., Smith R., Torralva B., Remington B.A., Schuh C.A., Jamarkani H., Meyers M.A. Appl Phys Lett 2006;88: 061917.
145 Jia D., Ramesh K.T., Ma E. Acta Mater 2003;51: 3495.
146 Koch C.C. Scr Mater 2003;49: 657.
147 Ma E. Scr Mater 2003;49: 663.
148 Fedorov A.A., Gutkin M.Yu., Ovid'ko I.A. Acta Mater 2003;51: 887.
149 Gutkin M.Yu., Kolesnikova A.L., Ovid'ko I.A., Skiba N.V. Phil Mag Lett 2002;82: 651.
150 Gutkin M.Yu., Ovid'ko I.A., Skiba N.V. Mater Sci Eng A 2003;339: 73.
151 Zghal S., Hytch S.J., Chevalier J-P., Twesten R., Wu P., Bellon P. Acta Mater 2002;50: 4695.
152 Bobylev S.V., Gutkin M.Yu., Ovid'ko I.A. J Phys D: Appl Phys 2004;37: 269.
153 Bobylev S.V., Gutkin M.Yu., Ovid'ko I.A. Acta Mater 2004;52: 3793.
154 Bobylev S.V., Gutkin M.Yu., Ovid'ko I.A. Phys Solid State 2004;46: 2053.
155 Wei Q., Jia D., Ramesh K.T., Ma E. Appl Phys Lett 2002;81: 1240.
156 Hasnaoui A., van Swygenhoven H., Derlet P.M. Phys Rev B 2002;66: 184112.
157 Shimokawa T., Nakatani A., Kitagawa H. Phys Rev B 2005;71: 224110.
158 Haslam A.J., Moldovan D., Yamakov V., Wolf D., Phillpot S.R., Gleiter H. Acta Mater 2003;51: 2097.
159 Liao X.Z., Zhou F., Lavernia E.J., Srinivasan S.G., Baskes M.I., He D.W., Zhu Y.T. Appl Phys Lett 2003;83: 632.
160 Chen M.W., Ma E., Hemker K.J., Sheng H.W., Wang Y.M., Cheng X.M. Science 2003;300: 1275.
161 Liao X.Z., Zhou F., Lavernia E.J., He D.W., Zhu Y.T. Appl Phys Lett 2003;83: 5062.
162 Wu X.L., Ma E. Appl Phys Lett 2006;88: 061905.
163 Wu X.L., Ma E. Appl Phys Lett 2006;88: 231911.
164 Zhu Y.T., Wu X.L., Liao X.Z., Narayan J., Mathaudhi S.N., Kecskés L.J. Appl Phys Lett 2009;95: 031909.
165 Udler D., Seidman D.N. Phys Rev B 1996;54: R11133.
166 Gutkin M.Yu., Ovid'ko I.A., Skiba N.V. Phys Solid State 2004;46: 2042.
167 Gutkin M.Yu., Ovid'ko I.A. Phil Mag 2006;86: 1483.
168 Bobylev S.V., Gutkin M.Yu., Ovid'ko I.A. Phys Rev B 2006;73: 064102.
169 Bobylev S.V., Gutkin M.Yu., Ovid'ko I.A. Phys Solid State 2006;48: 1495.
170 Liao X.Z., Srinivasan S.G., Zhao Y.H., Baskes M.I., Zhu Y.T., Zhou F., Lavernia E.J., Xu H.F. Appl Phys Lett 2004;84: 3564.
171 Bobylev S.V., Ovid'ko I.A. Rev Adv Mater Sci 2004;7: 75.
172 Zhu Y.T., Liao X.Z., Srinivasan S.G., Zhao Y.H., Baskes M.I., Zhou F., Lavernia E.J. Appl Phys Lett 2004;85: 5049.
173 Zhu Y.T., Liao X.Z., Srinivasan S.G., Lavernia E.J. J Appl Phys 2005;98: 034319.
174 Asaro R.J., Krysl P., Kad B. Phil Mag Lett 2003;83: 733.
175 Zhu B., Asaro R.J., Krysl P., Bailey R. Acta Mater 2005;53: 4825.

176 Gutkin M.Yu., Ovid'ko I.A., Skiba N.V. Phys Rev B 2006;74: 172107.
177 Gutkin M.Yu., Ovid'ko I.A., Skiba N.V. Phys Solid State 2007;49: 874.
178 Fischer F.D., Oberaigner E.R., Waitz T. Scr Mater 2009;61: 959.
179 Gu P., Kad B.K., Dao M. Scr Mater 2010;62: 361.
180 Zhao Y.H., Liao X.Z., Zhu Y.T., Horita Z., Langdon T.G. Mater Sci Eng A 2005;410–411: 188.
181 Huang C.X., Wang K., Wu Z.F., Zhang Z.F., Li G.Y., Li S.X. Acta Mater 2006;54: 655.
182 Feng X.Y., Cheng Z.Y., Zhou J., Wu X.L., Wang Z.Q., Hong Y.S. Chin Phys Lett 2006;23: 420.
183 Feng X.Y., Cheng Z.Y., Wu X., Wang T.C., Hong Y.S. J Phys D: Appl Phys 2006;39: 746.
184 Wu X.L., Qi Y., Zhu Y.T. Appl Phys Lett 2007;90: 221911.
185 Wu X.L., Ma E. J Mater Res 2007;22: 2241.
186 Wu X.L., Ma E., Zhu Y.T. J Mater Sci 2007;42: 1427.
187 Wu X.L., Ma E. Mater Sci Eng A 2008;483–484: 84.
188 Rösner H., Markmann J., Weissmüller J. Phil Mag Lett 2004;84: 321.
189 Wang Y.M., Hodge A.M., Biener J., Hamza A.V., Barnes D.E., Liu K., Nieh T.G. Appl Phys Lett 2005;86: 101915.
190 Zhu Y.T., Narayan J., Hirth J.P., Mahajan S., Wu X.L., Liao X.Z. Acta Mater 2009;57: 3763.
191 Rybin V.V. Large plastic deformations and fracture of metals. Moscow: Metallurgia; 1986 (in Russian).
192 Seefeldt M. Rev Adv Mater Sci 2001;2: 44.
193 Klimanek P., Romanov A.E., Seefeldt M., editors. Sol State Phenom 2002;87: 1.
194 Ke M., Hackney S.A., Milligan W.W., Aifantis E.C. Nanostruct Mater 1995;5: 689.
195 Murayama M., Howe J.M., Hidaka H., Takaki S. Science 2002;295: 2433.
196 Shan Z.W., Stach E.A., Wiezorek J.M.K., Knapp J.A., Follstaedt D.M., Mao S.X. Science 2004;305: 654.
197 Shan Z.W., Stach E.A., Wiezorek J.M.K., Knapp J.A., Follstaedt D.M., Mao S.X. Science 2005;308: 356d.
198 Shan Z.W., Mao S.X. Adv Eng Mater 2005;7: 603.
199 Sergueeva A.V., Mara N.A., Valiev R.Z., Mukherjee A.K. Mater Sci Eng A 2005;410–411: 413.
200 Sergueeva A.V., Mukherjee A.K. Rev Adv Mater Sci 2006;13: 1.
201 Sergueeva A.V., Mara N.A., Krasilnikov N.A., Valiev R.Z., Mukherjee A.K. Phil Mag 2006;86: 5797.
202 Yagi N., Rikukawa A., Mizubayashi H., Tanimoto H. Mater Sci Eng A 2006;442: 323.
203 Wang Y.B., Li B.Q., Sui M.L., Mao S.X. Appl Phys Lett 2008;92: 011903.
204 Zizak I., Darowski N., Klaumünzer S., Schumacher G., Gerlach J.W., Assmann W. Phys Rev Lett 2008;101: 065503.
205 Zizak I., Darowski N., Klaumünzer S., Schumacher G., Gerlach J.W., Assmann W. Nucl Inst Meth Phys Res B 2009;267: 944.
206 Feichtinger D., Derlet P.M., Van Swygenhoven H. Phys Rev B 2003;67: 024113.
207 Dupont V., Sansoz F. Mater Res Soc Symp Proc 2006; 903E:0903–Z06–05.1.
208 Sansoz F., Dupont V. Appl Phys Lett 2006;89: 111901.
209 Sansoz F., Dupont V. Mater Sci Eng C 2007;27: 1509.
210 Monk J., Farkas D. Phys Rev B 2007;75: 045414.
211 Gutkin M.Yu., Mikaelyan K.N., Ovid'ko I.A. Sov Phys Solid State 1995;37: 300.
212 Gutkin M.Yu., Mikaelyan K.N., Ovid'ko I.A. Nanostruct Mater 1995;6: 779.

213 Gutkin M.Yu., Mikaelyan K.N., Ovid'ko I.A. Phys Stat Sol B 1996;153: 337.
214 Gutkin M.Yu., Kolesnikova A.L., Ovid'ko I.A., Skiba N.V. J Metastable & Nanostruct Mater 2002;12: 47.
215 Gutkin M.Yu., Ovid'ko I.A., Skiba N.V. Tech Phys Lett 2002;28: 437.
216 Valiev R.Z., Langdon T.G. Acta Metall Mater 1993;41: 949.
217 Nyilas R.D., Kobas M., Spolenak R. Acta Mater 2009;57: 3738.
218 Ovid'ko I.A. Science 2002;295: 2386.
219 Gutkin M.Yu., Ovid'ko I.A., Skiba N.V. Acta Mater 2003;51: 4059.
220 Orlova T.S., Romanov A.E., Nazarov A.A., Enikeev N.A., Alexandrov I.V., Valiev R.Z. Tech Phys Lett 2005;31: 1015.
221 Orlova T.S., Nazarov A.A., Enikeev N.A., Alexandrov I.V., Valiev R.Z., Romanov A.E. Phys Solid State 2005;47: 845.
222 Enikeev N.A., Orlova T.S., Alexandrov I.V., Romanov A.E. Sol State Phenom 2005;101–102: 319.
223 Kolesnikova A.L., Ovid'ko I.A., Romanov A.E. Tech Phys Lett 2007;33: 641.
224 Romanov A.E., Kolesnikova A.L., Ovid'ko I.A., Aifantis E.C. Mater Sci Eng A 2009;503: 62.
225 Bobylev S.V., Mukherjee A.K., Ovid'ko I.A. Rev Adv Mater Sci 2009;19: 103.
226 Gutkin M.Yu., Ovid'ko I.A. Appl Phys Lett 2005;87: 251916.
227 Gutkin M.Yu., Mikaelyan K.N., Ovid'ko I.A. Scr Mater 2008;58: 850.
228 Gutkin M.Yu., Mikaelyan K.N., Ovid'ko I.A. Phys Solid State 2008;50: 1266.
229 Ovid'ko I.A., Sheinerman A.G., Aifantis E.C. Acta Mater 2008;56: 2718.
230 Bobylev S.V., Ovid'ko I.A. Rev Adv Mater Sci 2009;22: 39.
231 Ovid'ko I.A., Sheinerman A.G. Scr Mater 2008;59: 119.
232 Kim B.N., Hirada K., Morita K. Acta Mater 2005;53: 1791.
233 Yang F., Yang W. Scr Mater 2009;61: 919.
234 Mishra R.S., Valiev R.Z., Mukherjee A.K. Nanostruct Mater 1997;9: 473.
235 Mishra R.S., Valiev R.Z., McFadden S.X., Mukherjee A.K. Mater Sci Eng A 1998;252: 174.
236 McFadden S.X., Misra R.S., Valiev R.Z., Zhilyaev A.P., Mukherjee A.K. Nature 1999;398: 684.
237 Islamgaliev R.K., Valiev R.Z., Mishra R.S., Mukherjee A.K. Mater Sci Eng A 2001;304–306: 206.
238 Mishra R.S., Stolyarov V.V., Echer C., Valiev R.Z., Mukherjee A.K. Mater Sci Eng A 2001;298: 44.
239 Mishra R.S., Valiev R.Z., McFadden S.X., Islamgaliev R.K., Mukherjee A.K. Phil Mag A 2001;81: 37.
240 Valiev R.Z., Song C., McFadden S.X., Mukherjee A.K., Mishra R.S. Phil Mag A 2001;81: 25.
241 Padmanabhan K.A., Gleiter H. Mater Sci Eng A 2004;381: 28.
242 Padmanabhan K.A. J Mater Sci 2009;44: 2226.
243 Gutkin M.Yu., Ovid'ko I.A., Skiba N.V. J Phys D: Appl Phys 2003;36: L47.
244 Gutkin M.Yu., Ovid'ko I.A., Skiba N.V. Acta Mater 2004;52: 1711.
245 Gutkin M.Yu., Ovid'ko I.A., Skiba N.V. Phys Solid State 2005;47; 1662.
246 Ovid'ko I.A., Sheinerman A.G. Acta Mater 2009;57: 2217.
247 Haber J.A., Buhro W.E. J Am Chem Soc 1998;120: 10,847.
248 Valiev R.Z., Kozlov E.V., Ivanov Yu.F., Lian J., Nazarov A.A., Baudelet B. Acta Metall Mater 1994;42: 2467.
249 Jin M., Minor A.M., Stach E.A., Morris Jr J.W. Acta Mater 2004;52: 5381.

250 Soer W.A., De Hosson J.Th.M., Minor A.M., Morris Jr J.W., Stach E.A. Acta Mater 2004;52: 5783.
251 De Hosson J.Th.M., Soer W.A., Minor A.M., Shan Z., Stach E.A., Syed Asif S.A., Warren O.L. J Mater Sci 2006;41: 7704.
252 Jin M., Minor A.M., Morris Jr J.W. Thin Solid Films 2007;515: 3202.
253 Zhang K., Weertman J.R., Eastman J.A. Appl Phys Lett 2004;85: 5197.
254 Zhang K., Weertman J.R., Eastman J.A. Appl Phys Lett 2005;87: 061921.
255 Gai P.L., Zhang K., Weertman J. Scr Mater 2007;56: 25.
256 Liao X.L., Kilmametov A.R., Valiev R.Z., Gao H., Li X., Mukherjee A.K., Bingert J.F., Zhu Y.T. Appl Phys Lett 2006;88: 021909.
257 Pan D., Nieh T.G., Chen M.W. Appl Phys Lett 2006;88: 161922.
258 Pan D., Kuwano S., Fujita T., Chen M.W. Nano Lett 2007;7: 2108.
259 Gianola D.S., Van Petegem S., Legros M., Brandstetter S., Van Swygenhoven H., Hemker K.J. Acta Mater 2006;54: 2253.
260 Gianola D.S., Warner D.H., Molinari J.F., Hemker K.J. Scr Mater 2006;55: 649.
261 Gianola D.S., Mendis B.G., Cheng X.M., Hemker K.J. Mater Sci Eng A 2008;483–484: 637.
262 Legros M., Gianola D.S., Hemker K.J. Acta Mater 2008;56: 3380.
263 Fan G.J., Fu L.F., Qiao D.C., Choo H., Liaw P.K., Browning N.D. Scr Mater 2006;54: 2137.
264 Fan G.J., Fu L.F., Choo H., Liaw P.K., Browning N.D. Acta Mater 2006;54: 4781.
265 Fan G.J., Wang Y.D., Fu L.F., Choo H., Liaw P.K., Ren Y., Browning N.D. Appl Phys Lett 2006;88: 171914.
266 Fan G.J., Fu L.F., Wang Y.D., Ren Y., Choo H., Liaw P.K., Wang G.Y., Browning N.D. Appl Phys Lett 2006;89: 101918.
267 Brandstetter S., Zhang K., Escuadro A., Weertman J.R., Van Swygenhoven H. Scr Mater 2008;58: 61.
268 Kulovits A., Mao S.X., Wiezorek J.M.K. Acta Mater 2008;56: 4836.
269 Rupert T.J., Gianola D.S., Gan Y., Hemker K.J. Science 2009;326: 1686.
270 Hasnaoui A., van Swygenhoven H., Derlet P.M. Acta Mater 2002;50: 3927.
271 Schiøtz J. Mater Sci Eng A 2004;375–377: 975.
272 Farkas D., Frøseth A., van Swygenhoven H. Scr Mater 2006;55: 695.
273 Sansoz F., Molinari J.F. Thin Solid Films 2007;515: 3158.
274 Dupont V., Sansoz F. Acta Mater 2008;56: 6013.
275 Cahn J.W., Mishin Y., Suzuki A. Acta Mater 2006;54: 4953.
276 Zhou L., Zhou N., Song G. Phil Mag 2006;86: 5885.
277 Zhang H., Srolovitz D.J., Douglas J.F., Warren J.A. Acta Mater 2007;55: 4527.
278 Ivanov V.A., Mishin Y. Phys Rev B 2008;78: 064106.
279 Mompiou F., Caillard D., Legros M. Acta Mater 2009;57: 2198.
280 Caillard D., Mompiou F., Legros M. Acta Mater 2009;57: 2390.
281 Mishin Y., Asta M., Li J. Acta Mater 2010;58: 1117.
282 Li J.C.M. Phys Rev Lett 2006;96: 215506.
283 Malygin G.A. Phys Solid State 2008;50: 1032.
284 Malygin G.A. Phys Solid State 2009;51: 1814.
285 Lefebvre S., Devincre B., Hoc T. J Mech Phys Solids 2007;55: 788.
286 Li Z., Hou C., Huang M., Ouyang C. Comp Mater Sci 2009;46: 1124.
287 Shodja H.M., Davoudi K.M., Gutkin M.Yu. Scr Mater 2008;59: 368.
288 Davoudi K.M., Gutkin M.Yu., Shodja H.M. Scr Mater 2009;61: 355.
289 Davoudi K.M., Gutkin M.Yu., Shodja H.M. Int J Solids Structures 2010;47: 741.